Sensor Package Analysis and Simulation for Direct Sensor-to-Satellite Links

Mohammad J. AL-Saleh

Thesis submitted to the faculty of the
Virginia Polytechnic Institute and State University
in partial fulfillment of the requirements for the degree

Master of Science
in
Electrical Engineering

Dr. Amir I. Zaghloul, Chair
Dr. Luiz A. DaSilva
Dr. Scott F. Midkiff

November 29, 2007
Falls Church, Virginia

Keywords: Miniature Sensor, DSSS, MEMS, LEO Satellite
Circular Microstrip Patch Arrays

Sensor Package Analysis and Simulation for Direct Sensor-to-Satellite Links

Mohammad AL-Saleh

Abstract

This thesis investigates the design and the performance of low-power microsensors that communicate directly to a satellite or a constellation of satellites. Information is spread using pseudo noise (PN) or Barker codes. The sensors use a single circular microstrip patch element with a wide beamwidth or a miniature phased array antenna that continuously scans to access the satellite(s). The array beam is controlled with a beam-forming network (BFN), which contains 3 or 4-bit phase shifters, which can be made in micro-electro-mechanical systems (MEMS) or in monolithic microwave integrated circuits (MMIC). The antennas are designed using array simulation program called 'ARRAY' and the results are used in another simulation program called Advanced Design System (ADS) to simulate the whole sensor package that uses one of the antennas. The simulation results show that a sensor as small as 2.35 cm in diameter is able to send information with data rate of 1 kbps at bit error rate less than 10^{-5} to low-earth orbit (LEO) satellites with a transmitted power of 27.5 microwatts (-15.6 dBm).

Acknowledgments

I would like to take this opportunity to earnestly thank Dr. Amir I. Zaghloul, my advisor, for his patient guidance and support in making this work possible. I also wish to acknowledge the help of Eng.Wilfredo Rivas-Torres from Agilent Technical Support, who contributed to various aspects of this work. Lastly, I would like to thank the faculty of Virginia Tech for making the experience of graduate school enriching and fulfilling.

Contents

List of Figures

List of Tables

Chapter 1

Introduction

1.1 Motivation and Background

Communication or detection is needed in some unsafe places where no equipment or personnel can reach, e.g. close to volcanoes, in a nuclear activity area, active seismic area or behind enemy lines. Typical remote sensing techniques make it possible to collect data in inaccessible areas but not in non-cooperative environment as it usually requires fixed large equipment that can be easily discovered. Small transmitters are needed to transfer the information with a reliable, secured link.

This thesis constitutes the groundwork and the first step in a broader proposal to model, simulate, analyze, design, build, and test a sensor package that addresses the aforementioned need. This sensor will be too small to be easily discovered (as small as 8 cm^3). It will sense, transfer data to digital bits, encode the message, up-convert to appropriate radio frequency (RF) and send it to low-earth-orbiting (LEO) satellites using phased array antenna that continuously scans its narrow beam to access the available satellite.

The goal of the design is to make as small sensor package as possible so it cannot be easily discovered. The sensor will use satellite links where line of sight is almost always available and the probability of receiving the information by a spy receiver is very low. The project consists mainly of two parts: the design of the sensor transmitter up to the antenna, and the design of the phased array antenna. The whole transmitter will be tested through simulation to make sure that its performance meets the required specifications.

The design of the transmitter from the analog-to-digital (A/D) converter up to the antenna, was done using the circuit simulation package Advanced Design System (ADS), while the design of the phased array antenna was conducted using the software ARRAY. The whole system then was tested by ADS again using a simulated line of sight link and a satellite receiver. Real practical numbers for each component parameters were collected from the industry and the literature and used in the simulation.

1.2 Sensors Mission Scenario

The sensors are dropped or otherwise positioned in the non-cooperative environment and start detecting the required parameters. The sensors will operate independently and may relay the same information to create a built-in redundancy. The damage or discovery of some of the sensor packages will not affect the transfer of the required information, as the remaining sensors will transmit the same information. The sensors use scanning antennas to access the satellite(s) from the randomly located sensors. The antennas have hemispherical coverage that can be achieved using small phased arrays with relatively high gain and narrow beamwidth, operating at a high frequency, such as Ka band (27-40 GHz). The array beam is controlled with a beam-forming network (BFN), which contains multiple-bit phase shifters; all can be made in micro-electro-mechanical systems (MEMS) or in monolithic microwave integrated circuits (MMIC). The medium for the BFN and phase shifters can be coplanar waveguides for compactness. The built-in control circuit will control the phase shifters to dynamically scan the array beam at the proper rate, without the need to track the satellite using acquisition and tracking mechanisms. A digital beam-forming chip can also be designed to facilitate the beam scanning. The array beam is continuously scanned within the expected look angle range to the satellite(s) with a pre-set dwell time at each scanning position, and transmits the coded sensor data in all scanning directions, as shown in Figure 1.1.

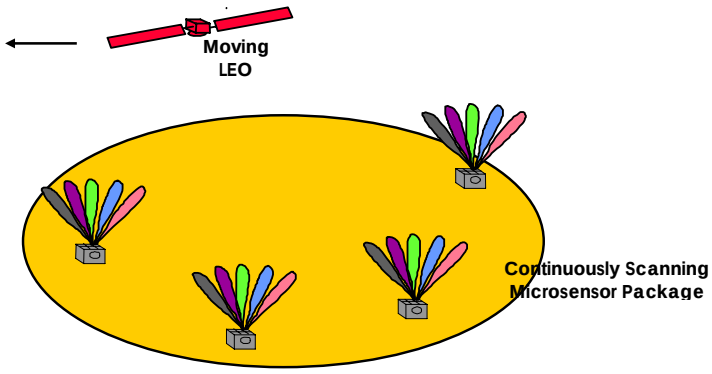

Figure 1.1: Direct sensor-to-satellite link using scanning phased arrays

The moving LEO satellite(s) will receive the data when the array beam is in the direction of the satellite(s). This data acquisition by the satellite is performed without the need for satellite tracking by the sensor. The hemispherical coverage can also be achieved through a low-gain hemispherical-beam antenna at L band (1-2 GHz), in which case the sensor power has to be enough to compensate for the low gain of the antenna. The low gain antenna solution is appropriate for lower frequency of operation.

1.3 Objective

This thesis aims to model, simulate, and analyze the operation of a miniature sensor package that transmits an encoded data from non-cooperative environments to satellites. The package uses a continuously scanning phased array and miniature transit components in a camouflaged enclosure. Redundant packages are thrown in the field for high reliability.

1.4 System Overview

The sensor package has two major components: the transmitter and the antenna. The transmitter starts with the sensing part which is basically a transducer. An analog-to-digital converter will follow the transducer to convert the information to digital format 0's and 1's. As in many of the satellite communication systems, binary phase shift keying (BPSK) will be used as the modulation scheme. A correlator will then spread the BPSK signal with one of the following codes: PN sequence, Barker or Kasami codes. Multiple up-converting stages will transfer the frequency from the intermediate frequency (IF) to the RF stage. The array will continuously scan the beam and transmit the sensor information such that the LEO satellites will pick up the signal during their path over the sensor field. At the satellite receiver, the signal will be filtered and amplified and then down-converted to the IF stage where decorrelation with the stored sequence of the used code will be conducted to recover the transmitted bits. The simulation ADS will then measure the bit error rate (BER) by applying the proper delay to the original bits and comparing them with the recovered ones.

The phased array antenna has a hexagonal shape with number of elements that extends from one element at L band up to 37-elements at Ka band. Each element is a circular microstrip patch with half-wavelength spacing between the elements.

1.5 Thesis Overview

This chapter provided an introduction to the work presented in the following chapters.

Chapter 2 presents a literature review about the major topics covered in the thesis. It starts by defining the 'sensing' process and listing the latest sensors applications. Then it discusses the array theory used in designing the sensor's antenna. The chapter talks about all the parameters used in designing microstrip antennas. Then it discusses the satellite orbit specifications and the modulation schemes used in satellite communication.

Next, the chapter discusses some existing detection systems. Types of links used (satellite links, microwave links) or via sensor networks and the performance of each type will be also discussed. Size, cost, and material used are all critical issues that are also discussed. Finally, typical barriers for practical use and the fabrication process such as low data rate, high cost, short life, low reliability and large physical size will be analyzed for each case.

Chapter 3 discusses the method used to design, simulate, build and test the whole sensor package. It starts by discussing the transmitter design process step by step from the sensing part to the antenna input. Then the chapter discusses the satellite receiver function and show how the performance is measured at the receiver end. It then talks about designing the antenna and how some dBs were gained in the link budget by using a high gain phased array antenna in the sensor, and how that saved the transmitted power and resulted in a small size sensor. The chapter will also explain why the Ka band was chosen for use in this application. Full parametric study will give the optimized design parameters (transmitter power, antenna gain, code length). The discussion shows the simplicity of the transmitter side by using fixed scanning steps to search for the available satellites. No acquisition or tracking mechanisms are needed. The coded signal will be studied as well as how it adds more dBs in the carrier-to-noise ratio in the link and at the same time secures the link. In general, chapter 3 discusses and analyzes the circuit components, and the antenna parameters, the material used to build RF components.

Chapter 4 talks about the detailed design of the three antennas proposed. It shows the parameters and the performance of each case followed by a comparison between the three cases. Next the antenna beam scanning process in 2-D and 3-D will be shown in

figures and explained in the discussion. Comparison between literature values and our simulation results is provided and finally the chapter briefly discusses the fabrication process for printing these antennas and the material used for that.

Chapter 5 presents the sensor design and the whole system simulation using ADS software package. The design is discussed component by component for both the transmitter and the receiver. For each component, the chosen parameters are discussed. Chapter 5 also relates theoretical formulas to the values used for each component and explains why every parameter was chosen. The signal will be tracked from the (A/D) to the output of the satellite receiver.

Chapter 6 presents extensively the simulation results for one of the proposed cases. The signal is plotted at each stage in the transmitter and the receiver. Every change the signal goes through is explained and compared to the expected results, and then the chapter provides the performance of the sensor at the used parameters and compares them by the theoretical values from the link budget calculations. Finally it mentions some necessary fabrication requirements and discusses the effect of some unused parameters that can be used in designing this sensor package.

Chapter 7 lists the major conclusion points and the future work as well as other possible applications of the designed sensor package.

Chapter 2

Review of Sensors and System Components

This chapter gives a brief literature review about the major topics of the sensor package design. Section 2.1 defines the 'sensing' process and provides some examples of typical sensors and shows how they work. Sections 2.2-2.5 discuss the array theory used in designing the sensor's antenna and the parameters used in designing the microstrip antennas. The satellite orbit specifications along with the modulation schemes used in satellite communication are discussed with examples on each type in sections 2.6 and 2.7. Section 2.8 discusses one of the existing detection systems that use sensors and satellite links.

2.1 Sensors

A sensor is an electrical device that detects information from the surrounding area then translates it to an electrical output as voltage or current. Sensors change one form of energy into another. They can detect, for example, temperature, gases, vibration, light, smoke, nuclear radiation and so their applications include machines, aerospace, automobiles, medicine, industry, and robotics. In the last decade, MEMS technology has enabled the development of low-loss, inexpensive wireless sensors with total volumes ranging from few cubic mm to several cubic cm. MEMS enables these devices by reducing both the volume and energy consumption of various components [1].

More sensor applications are provided every day because of the flexibility of using them. They can be left without monitoring. They are usually fabricated with low cost so users can use many of them for reliability. They are so small so they can reach places where other typical electronic devices cannot reach such as the case in the medical application. They can communicate with each other and survive in very high or low temperatures.

The requirement of both evolutionary and revolutionary advances in miniaturization, integration, and energy management of these sensors has engendered a new generation of very small sensors called "Smart Dust". Smart dust was introduced by Kristofer S. J. Pister (University of California - Berkeley) in 2001 [2]. Smart dust is a

hypothetical network of tiny wireless MEMS sensors, robots, or devices, installed with wireless communications that can detect (for example) light, temperature, or vibration. Dr. Pister's group at UC Berkeley has been using smart dust in deploying defense networks rapidly by unmanned aerial vehicles or artillery, monitoring rotating compression-blade high-cycle fatigue, tracking the movements of birds, small animals, and insects, providing interfaces for the disabled and many other applications. Figure 2.1 shows their conceptual diagram of the Smart Dust mote that was proposed in 2001. According to [2], they can be supplied with power from a hick-film battery or a solar cell with charge-integrating periods of darkness, or both. The design can be integrated to be used in many applications including light, temperature, magnetic field, and acoustics. The transmitter can be passive using a corner-cube retroreflector, or active using a laser diode and steerable mirrors which consumes 1 joule per bit.

One of the major limitations of this design was the used antenna. Two choices were available: the RF antenna or the optical one. While an antenna at Radio-Frequency would be very large to fit in the Smart Dust, an optical antenna was the left choice. An optical antenna or lens, will give a much higher gain than the antenna at RF frequencies with the same size. Nevertheless, optical antennas have some drawbacks. The short range, the line of sight requirement and the beam pointing accuracy were the major limitations that stimulated us to find new methods for effective transmission for long distances while keeping the sensor as small as possible.

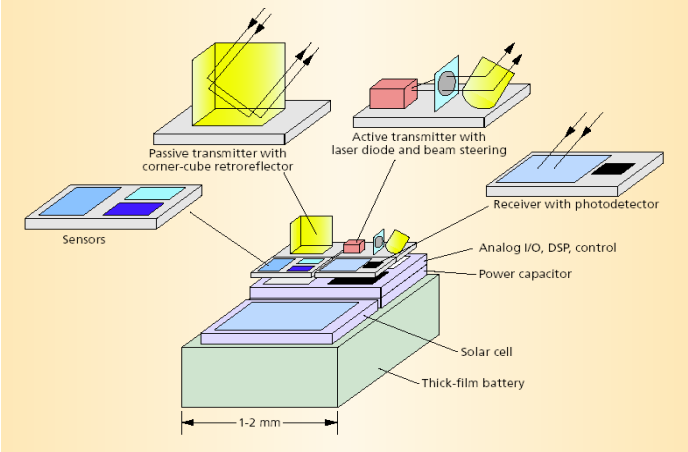

Figure 2.1: Conceptual diagram showing a Smart Dust mote's major components. (© 2002 IEEE) Reprinted, with permission from IEEE, from [1]

2.2 Array Theory

A phased array is a group of antennas in which the relative phases of the respective signals feeding the antennas are varied in such a way that the effective radiation pattern of the array is reinforced in a desired direction and suppressed in undesired directions [3].

Phased array antennas are able to electronically steer the beam in angle by changing the phase of the current at each element. The electronic beam steering replaced the old difficult mechanical steering of large and heavy antennas. Nevertheless, mechanical and electronic steering is combined in some applications for 3-D target tracking. Phased arrays advantages are many: they can provide rapid beam-steering, multi-targets tracking, lower radar cross section if properly designed, and convenient shape for flush mounting or for blast hardening [4]. Phased arrays are used in radar systems in target tracking and detection. The main disadvantage that still exists and restricts the use of these antennas to military applications is the complexity and high cost.

Phased Arrays can be found in two classes: conformal arrays and planar arrays.
A conformal array antenna is a three-dimensional configuration of antenna elements that conforms to something; it conforms to a prescribed shape. The shape can be some part of an airplane, high-speed train, ship, or other vehicle. The purpose of the conformal array is to build the antenna so that it becomes integrated with the structure and does not cause extra drag. The purpose can also be that the antenna integration makes the antenna less disturbing, less visible to the human eye; for instance, in an urban environment can be flush-mounted on the exterior of the aircraft surface [5].

A planar array is a two-dimensional configuration of antenna elements arranged to lie in a plane. Planar arrays can be also classified, depending on the direction of the maximum radiation, e.g. broadside array and an endfire array. A broadside array is an antenna with a maximum radiation direction perpendicular to the plane of the antenna. Figure 2.2 shows one of the largest planar arrays used in defense radar systems used by the US air force.

Figure 2.2: 90-foot diameter planar phased array - Alaska - Clear Radar Upgrade program (Photo courtesy of Alaska District)

An endfire array is the one with a maximum radiation direction parallel to the plane of the antenna. Figure 2.3 demonstrates the two array patterns, broadside and endfire.

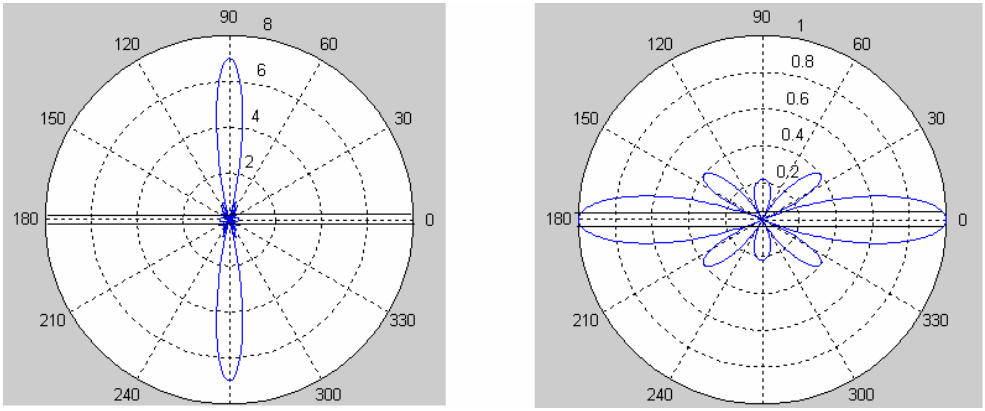

Figure 2.3: (Left Side) Broadside array pattern. (Right Side) Endfire array pattern

Similar elements also can have similar orientation or dissimilar orientation. All of that depends on the function and the radiation pattern needed from the antenna. The radiation pattern of an array of identical elements is the product of two parts- the pattern of each individual element (called the element pattern), and the array pattern that would result if the elements were isotropic radiators (also called the array factor).

$$F(\theta, \varphi) = g_a(\theta, \varphi)\, f(\theta, \varphi) \qquad (1)$$

where F (θ, φ) is the overall, normalized pattern of the array, g_a (θ, φ) is the normalized element pattern, and f (θ, φ) is the normalized array factor.

Pattern multiplication is fundamental to the operation of arrays; however, it is not applicable to arrays comprised of elements with dissimilar orientations, since the factorization of the overall pattern into the element and array factors is then not possible.

2.3 Circular Microstrip Patch Antennas

A microstrip patch antenna consists of two parallel conductors separated by a thin layer of dielectric substrate. The lower conductor functions as a ground plane and the upper conductor acts as a patch antenna. Figure 2.4 shows is a typical circular microstrip patch antenna with radius R, substrate thickness h, and a dielectric relative permittivity ϵ_r.

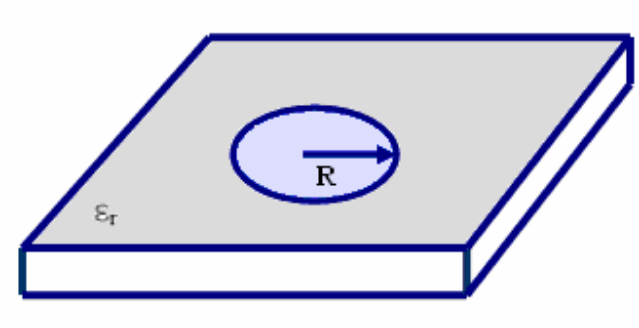

Figure 2.4: Circular microstrip patch antenna

Microstrip patches can be square, rectangular, circular, triangular, elliptical, or any other common shape to simplify analysis and performance prediction.

Microstrip antennas have several advantages, such as low cost, ease of construction, low profile design, and suitability in conformal array applications. However, microstrip antennas have low bandwidths, typically only a few percent. Since microstrip antennas are resonant in nature, their required size becomes inconveniently large at lower frequencies. They are thus typically used at frequencies between 1 and 100 GHz. Microstrip antennas are relatively low-gain antennas. Their end-fire radiation characteristics and power-handling capability are relatively poor.

Microstrip antennas radiate due to the fringing fields between the patch and the ground plane. Figure 2.5, shows the fringing fields in a microstrip patch antenna.

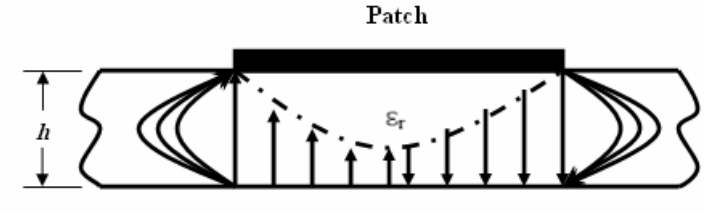

Figure 2.5: Fringing fields in microstrip antenna

Multiple modes can be excited in a circular microstrip patch antenna, and the resulting far field electric field θ and φ components can be shown to be as follows [6]:

$$E_\theta^{(n)} = e^{jn\pi/2} (V_0^{(n)} / 2)\ k_0 R (J_{n+1} - J_{n-1}) \cos n(\varphi - \varphi_0)$$
$$E_\varphi^{(n)} = -e^{jn\pi/2} (V_0^{(n)} / 2)\ k_0 R (J_{n+1} + J_{n-1}) \cos\theta \sin n(\varphi - \varphi_0) \qquad (2)$$

In these equations, V_0 is the input voltage, k_0 is the wavenumber, $J_n = J_n (k_0 R \sin\theta)$ is the Bessel function of the second kind and order n, R is the radius of the patch, and φ_0 is the angle corresponding to the feeding point of the antenna.

Due to the fringing fields between the patch and the ground plane, the effective dimensions of the antenna are greater than the actual dimensions. The effective radius of the patch is related to the physical radius of the patch by [7]:

$$r_{eff} = R [1 + (2h /(\pi R \varepsilon_r)) \{\ln(R/(2h)) + (1.41 \epsilon_r + 1.77) + (h/R) (0.268\epsilon_r + 1.65)\}]^{1/2} \qquad (3)$$

where R is the physical radius of the patch and h is the height of the dielectric substrate.

The resonant frequency of a microstrip patch antenna is dependent on the effective patch radius, and is given by [7]:

$$f_r = \frac{c.a_{nm}}{2\pi.r_{eff}.\sqrt{\varepsilon_r}} \qquad (4)$$

where c is the velocity of light, r_{eff} is the effective radius of the circular patch, and α_{nm} are the zeros of the derivative of the Bessel function $J_n(x)$. m and n specify the mode that is being considered. For the fundamental resonating TM_{11} mode, for example, the above equation produces [7]:

$$f_r = \frac{1.8412c}{2\pi . r_{eff} . \sqrt{\varepsilon_r}} \quad (5)$$

2.4 Microstrip Arrays

Microstrip patch antennas are inherently low-gain antennas and this fact partially offsets the advantages they offer in terms of cost and ease of fabrication. They offer the advantage that the elements can be printed easily and at low cost on a flexible dielectric substrate. However, microstrip patch antennas are practically well suited from a technological point of view to be grouped in large arrays to obtain high gain. Such arrays are ideally suited for any application that calls for the design of low-profile, conformal antennas. Additionally, microstrip radiating elements along with the feed networks can be integrated with the transmitting and receiving circuitry. Typically, the feed lines are integrated on the same substrate. It may also be possible to integrate active devices for phase shifters and pre-amplifiers on the same substrate, or on a lower layer supporting the active elements that has a different permittivity better suited to the active elements [8]. Figure 2.6 shows a planar array using circular microstrip patch elements.

Figure 2.6: Planar array of circular microstrip patches in circular configuration

2.5 MEMS Technology

MEMS or micro-electro-mechanical systems is the integration of mechanical elements, sensors, actuators, and electronics on a common silicon substrate through microfabrication technology. MEMS technology can be implemented using Silicon,

polymers or metals, the choice of which will depend on the device being created and the market sector in which it has to operate. MEMS technology is allowing the development of smart products, augmenting the computational ability of microelectronics with the perception and control capabilities of microsensors and microactuators and expanding the space of possible designs and applications. MEMS offers the benefits of significantly reduced mass and power consumption translating directly into direct cost benefits as a result of the major decrease in size as shown in the example in Figure 2.7. Its applications include Biotechnology, communication and many others. In sensors industry, MEMS allows complex electromechanical systems to be manufactured using batch fabrication techniques, decreasing the cost and increasing the reliability of the sensors and actuators to equal those of integrated circuits. Yet, even though the performance of MEMS devices is expected to be superior to macroscale components and systems, the price is predicted to be much lower [9].

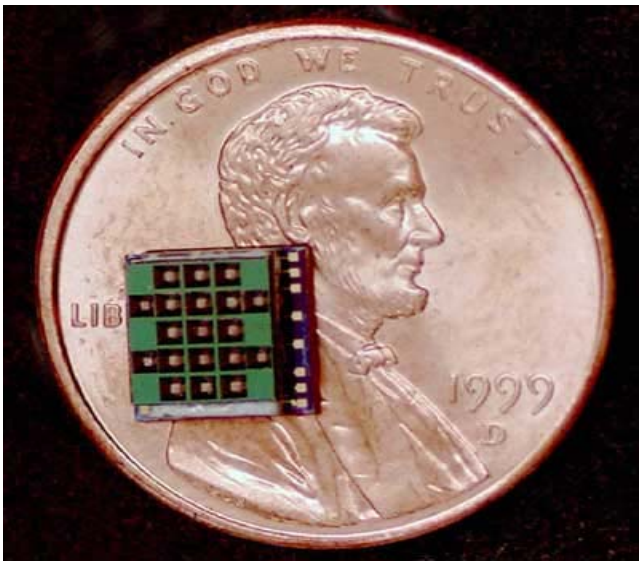

Figure 2.7: TRW prototyped digital propulsion Microthruster. This microthruster contains 15 individual thrusters in the central 3x5 array. Photo Courtesy of TRW

2.6 Satellite Orbits

Satellites are classified by their orbital altitudes: low earth orbit (LEO), medium earth orbit (MEO), geostationary (GEO) and high earth orbit (HEO) [10].

Low earth orbit (LEO) satellites have orbital altitudes between 200 km and 2000 km, which is the lowest usable range of orbital altitudes. The altitude is usually not less than 300 km because that would be impractical due to the larger atmospheric drag. LEO satellites are often used for communication systems because they require lower transponder output power. Examples of LEO satellite systems include IRIDIUM and Globalstar.

Medium earth orbit (MEO) satellites have orbital altitudes between 2,000 km and 35,786 km. MEO satellites are also referred to as intermediate circular orbit (ICO) satellites. MEO is used mainly for navigation, such as the American GPS at 20,200 km, the Russian Glonass at 19,100 km, and the European Galileo at 23,222 km.

Geostationary satellites appear motionless in the sky by orbiting the Earth at the same angular velocity as the Earth's rotation. Therefore, the orbital period of a geostationary satellite is equivalent to sidereal one day. The altitude required to achieve this orbital period is 35,786 km. GEO satellites are preferred for communication systems because an antenna can point in a fixed direction and maintain a link with the satellite. Examples of satellite communication systems in geostationary orbit include imagery, television, and communication.

High Earth Orbit (HEO) satellites have orbital attitudes above the altitude of geosynchronous orbit 35,786 km (22,240 miles). Due to the very high altitudes used, HEO orbits are best used in polar coverage. They provide the longer dwell time as well for the same reason.

2.7 Spread Spectrum

Spread spectrum is the method in which energy generated in a particular bandwidth is deliberately spread in the frequency domain, resulting in a signal wider in bandwidth. Spread spectrum techniques are used for a variety of reasons, including the establishment of secure communications, increasing resistance to natural interference and jamming, or to prevent detection. Spread spectrum can be implemented by two ways:

1) Direct Sequence Spread Spectrum (DSSS): where the message is multiplied by high speed *chip* sequence and the resulted signal occupies the full bandwidth all the time. Examples are the GPS and most of the military communications. The chipping code in

the DSSS technique is a redundant bit pattern for each bit that is transmitted, which increases the signal's resistance to interference. If one or more bits in the pattern are damaged during transmission, the original data can be recovered due to the redundancy of the transmission.

2) Frequency Hopping (FH): where the transmitter changes frequency in random sequence and keeps 'hopping' across the available bandwidth. FH is rarely used in satellite links but can be found in applications like Bluetooth.

At the transmitter side, the transmitted signal is spread over a frequency much wider than the minimum bandwidth required to send the signal. Figure 2.8 shows the spreading and the despreading process at the transmitter and the receiver sides. DSSS code division multiple access (CDMA) uses Pseudo Noise (PN) codes which appear random and have a flat spectrum that will look like noise unless the right code is used at the receiver side.

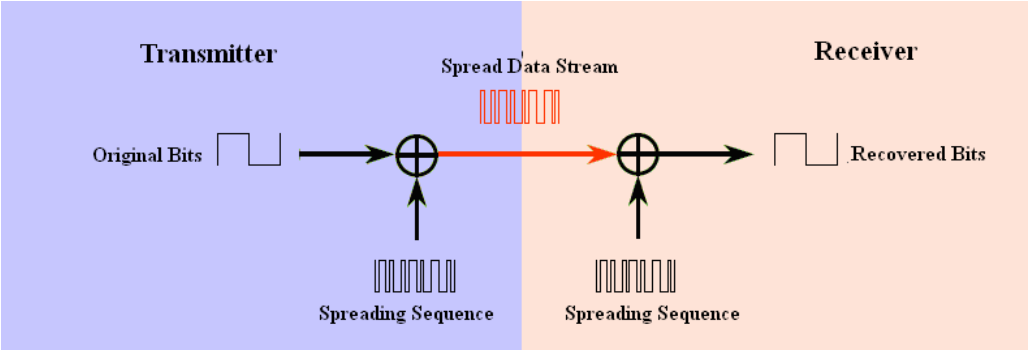

Figure 2.8: Spreading and despreading process

At the receiver side, the received spread spectrum signal is multiplied by the chip sequence to recover the message signal, the process which is known as *correlation.* If the right code is used, the receiver integrator will have a finite output, otherwise the output will tend to zero. Figure 2.9 shows how despreading with the right code sequence extracts the buried message (in blue) signal from the noise (in pink).

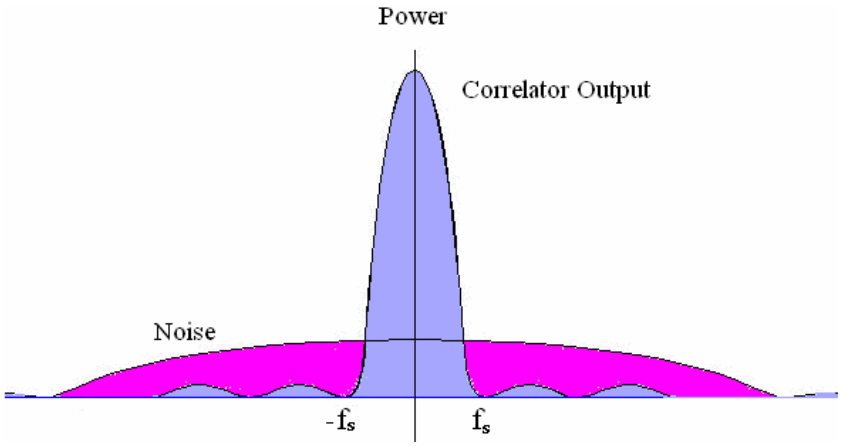

Figure 2.9: Correlation with the right code

Codes are usually very long. PN (m) sequence, Gold, or Kasami codes are the most popular codes used in satellite and GPS links. These codes are not quite orthogonal, but close enough. Two or more of these codes can be multiplied for improved performance. GPS uses Gold codes by multiplying two PN sequences to generate a very long code for high security.

2.8 Similar projects

This section discusses a similar project done by other researcher:

-'An Application of a Disposable Remote Chemical Sensor Network':

This paper [11], discussed the technical consideration of the design of a disposable remote chemical sensor network. It started by talking about the different procedures of sensing the presence of chemical agents or hazardous chemicals.

Communication link: Communication between these chemical sensors and the land-based transponder can be done by three procedures: via a terrestrial communication link, through an airborne transponder or via LEO satellites. Due to the multipath fading and the easy detection, the first option was removed. Option number two shares the detection problem with the first one but not the multipath problem. LEO satellites do not have any of these problems and, in general, are more reliable way of communication. The reason of why the author proceeded with the assumption that LEO satellites would be

used for communication. An orbit of altitude 250 km was selected. With an elevation angle of one degree, the slant range would be 1803.2 km.

Antenna: For the LEO satellite, a quadrifilar helix antenna was chosen because of its light weight, relative small size, hemispheric pattern and the fact that it does not have ground plane. For the remote, the same requirements were needed. In addition, the antenna should be appropriate for directive patterns and circular polarization. One of the antennas that were found to have all of that is the axial mode helical antenna.

Data Rate: No certain data rate was assumed but the data rate was supposed to be very low since the sensor would be only 'telling' the satellite if there is or is not chemical activity around it. The message, for example, would have two bits to indicate if the threshold is exceeded, 15 bits to tell about the faults in the sensor and some bits to identify the sensor for the receiver.

Access Technique: Three access methods were examined: random access, direct sequence CDMA, and adaptive polling with random burst transmission. From a complexity and cost point of view, DS CDMA was the most expensive and complicated system. DS CDMA requires more bandwidth than frequency hopping (FH) and random burst (DAMA). Moreover, DS CDMA is typically implemented with coherent demodulation which is not needed at FH CDMA or random burst DAMA. On the other hand, FH CDMA requires a frequency synthesizer that is adept at switching carrier frequencies very rapidly. FH as well as DS CDMA receivers should acquire and track the (PN) code.

Modulation: As in most of the low data rate applications, BPSK was a typical choice as it is one of the most power-efficient digital modulation techniques and suitable for simple designs.

Power Source: A Lithium battery with two or three Watts was suggested. Such batteries with less than fifty percent duty cycle were considered by [12] a good choice for this application.

Frequency Bands: Table 2.1 lists the frequency bands used for down and uplinks:

Table 2.1: Uplink and downlink frequency bands

Tx \ Rx	LEO Sat	Hub	Sensor
LEO Sat	----------	2650 MHz - BPSK	400.13 MHz - FSK
Hub	2685 MHz - FSK	----------	----------
Sensor	469 MHz - BPSK	----------	----------

Summary and discussion of the results: The author provided many possible options to fully design a small disposable chemical sensor. The proposed method uses LEO satellite orbits to receive the information on the UHF band and retransmit it to a fixed hub. Low data rate was needed with an omnidirectional antenna. The proposed design wouldn't give a secure link but the link would be so resistant to jamming and encryption. Directive antenna was suggested to solve this problem, but the penalty would be more complex and expensive system.

The need for secure link was one of the motivations of our work presented in this thesis. Next chapter presents the steps of setting the design major parameters and explains how each chosen parameter is related to the final performance and the design requirements.

Chapter 3

System Aspects of Sensor-to-Satellite Link

This chapter discusses the transmitter-receiver design process step by step. It explains how and why each parameter was chosen. Section 3.1 talks about the transmitter parameters which are used in designing the sensor. Section 3.2 discusses the satellite receiver components and then goes through the reverse engineering process used to determine the minimum transmitted power based on the desired performance of the whole system.

3.1 Transmitter Subsystem

3.1.1 Satellite Communication Frequencies

World Radio Conferences have allocated the L, S, C, Ku, K, Ka, V and Q frequency bands for commercial satellite services [13]. As LEO satellites were more interesting because they are the closest to the Earth, the research started by considering the L band which is the most used band in LEO systems. Trying to achieve the goal of building an antenna of aperture size that does not exceed 10 cm^2, it was found impossible to use the L band unless a larger sensor package is considered as well. The alternate solution was to go to a higher band which results in a higher path loss. Frequency Bands above the Ka band suffer from high path loss. Ka band was found to be the best choice as it is the optimum point between the path loss, the antenna size and the circuit cost. On the other hand, L band showed a lower path loss and resulted in simpler but larger antenna as shown in the antenna section.

3.1.2 Sensing Process

The Sensing process depends on the application of the sensor. Light sensors which are typically PIN diodes are by far the most commonly used type of light meters in lighting systems. The principle, on which they detect incident light, is based on electron photo excitation effect, which causes increase of electrical current through the diode [14].

Temperature sensitive resistors or 'thermistors' measure temperature changes, relying on the change in its resistance with changing temperature. Image sensors produce images by capturing light and converting it into electrical signals. In the electrochemical sensing method, chemical vapors are usually ionized via a radioactive source. The ionized vapors then pass through an electromagnetic field, where different chemicals are distinguished according to their differences in electrical charge and resulting characteristic residence times in the electromagnetic field [11].

Whatever the application of the sensor, the process is the same. They change one form of energy into electrical output. This output is usually an analog voltage and so followed by (A/D) if digital communication is used. The sensing process explained so far is outside the scope of the thesis. This step was skipped in the simulation and instead random bits were generated to represent the sensor data at the output of the (A/D).

3.1.3 Modulation and Coding

Typical satellite communication systems use one of the fundamental modulation techniques: Binary phase shift keying (BPSK); quadrature phase shift keying (QPSK); orthogonal quadrature phase shift keying (OQPSK); 8-PSK; and quadrature amplitude modulation (QAM), especially 16-QAM. The higher data rate systems usually use higher capacity modulation techniques such as 8-PSK or 16-QAM but with higher probability of bit error (BER) penalty. For low data rate systems, techniques like BPSK and QPSK are more preferred because of their simplicity and low cost of implementation.

Wireless sensor output data rate is usually 50 – 10000 bps. As the goal was to build a low-cost simple system, with a data rate that does not exceed 10 kbps, BPSK was found to be the best choice in addition to its high power efficiency. Another reason that helped deciding was using DSSS in the sensor to encode the signal.

In the designed sensor, DSSS is used with the long PN-Sequences or the short Barker codes. Using spread spectrum with such codes gave two main advantages: 1) Coding gain which reduced the required transmitted power. 2) The information was 'encrypted' by using such codes. Since the ADS simulation didn't have any Barker code, up to the date of writing this thesis, in its CDMA library, only theoretical values of the Barker coding gain were used which is defined as:

$$Coding\ Gain\ (dB) = 10\ Log_{10}\ (Code\ Length) \quad (6)$$

The satellite receiver uses a delayed version of the transmitted bits to decorrelate with the received ones and the output is then filtered and applied to a component that measures the BER by trying hundreds of samples.

3.2 Receiver Subsystem

3.2.1 Performance

As the application in this project is considered a safety application, a reliable communication link with low error rate was required. The design procedure started with a goal of final BER of less than 10^{-5}. This value was enough because the assumed data rate didn't exceed 10 kbps. Lower BER could be obtained by changing any of the primary elements.

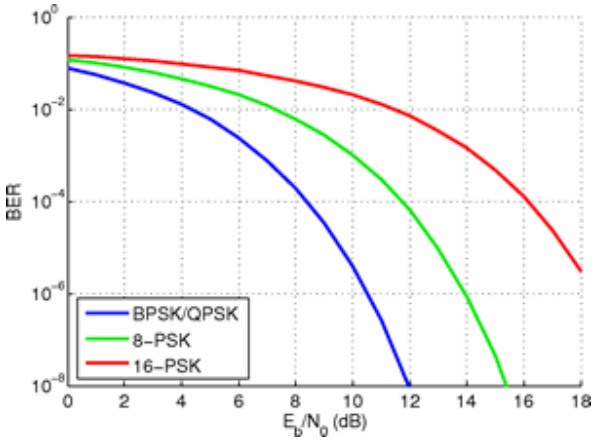

Figure 3.1: BER vs. Eb/No for PSK

From Figure 3.1 or from the tables in [13], the required (E_b/N_o) for the BPSK case was found to be 9.9 dB. According to [13], a 0.5 dB margin is considered enough for such systems with low data rate. Satellite engineers usually use a higher margin to cover all the RF losses. Our sensor didn't include many lossy RF components so a total margin of 3 dB was assumed to cover all other unconsidered losses. The required (E_b/N_o) became 12.9 dB.

To attain the desired BER at the receiver end, it was necessary to study all the factors that control this value. For the coherent BPSK used in this system, the (E_b/N_o) is defined as [13]:

$$(E_b/N_o) = (C/N).\ (B/R_b) \qquad (7)$$

where (C/N) is the carrier to noise power ratio at the receiver end, B is the last stage bandwidth, and R_b is the data rate of the transmission. Equation (7) shows that E_b is a function of the received carrier power and the data rate, and that N_o is a function of the thermal noise at the final stage and the bandwidth of that stage. Thermal noise was considered to be the dominating source of noise and can be defined as:

$$Noise = k.\ T_s.\ B \qquad (8)$$

where k is Boltzmann's constant =1.3806504 $\times 10^{-23}$ J/K or -228.6 dBW/K/Hz [13], T_s is the physical temperature of system in Kelvin degrees and B is the noise bandwidth in which the noise power is measured, in Hertz. In the design of the satellite receiver, the receiver has a typical system temperature of 500 Kelvin, a value which many commercial satellites use in their receivers [13]. Using equation (8) above, the theoretical received signal level at the satellite was determined.

Table 3.1 shows the results of the power study for two data rates: 500 and 1000 bps.

Table 3.1: Power study at the satellite receiver end

E_b/N_o (theoretical) - dB	9.9	9.9
E_b/N_o (with margin) - dB	12.9	12.9
Noise temperature T_s - Kelvin	500	500
Receiver Noise Figure (NF) - dB	4.4	4.4
Noise spectral density (N_o) - dBW/Hz	-199.6	-199.6
Energy per bit (E_b) - dBJ	-186.7	-186.7
Information Data Rate - bps	500	1000
Received Signal Level (RSL) - dBW	-159.7	-156.7

Calculating the minimum received signal level for each data rate was necessary to determine other important parameters like the transmitted power, code length needed and others.

3.2.2 Link Budget

A satellite antenna gain of 20 dB which corresponds to almost 20 degree of beamwidth was assumed. This value along with the path loss enabled was used to determine the minimum effective isotropic radiated power (EIRP) from the link budget equation [13].

$$P_r\,(dB) = P_t + G_t + G_r - Path\ Loss \qquad (9)$$

where EIRP is defined as the product of the transmitted power (P_t) in watts with the transmitting antenna gain in ratio, and the Path Loss is:

$$Path\ Loss\ (dB) = 20Log_{10}\frac{\lambda}{4\pi.d} \qquad (10)$$

where d is the range to the satellite and λ is the wavelength.

Using equations (9) and (10), the minimum EIRP for the sensor transmitter was calculated. Table 3.2 shows the minimum values needed for the cases of the 780 and 1410 km links with data rates of 500 and 1000 bps at uplink frequency of 30 GHz

Table 3.2: Uplink power budget

Data Rate - bps	500		1000	
Received Signal Level - dBW	159.7	-159.7	-156.7	-156.7
Satellite Antenna Gain - dB	20.0	20.0	20.0	20.0
Satellite Altitude - km	1410	780	1410	780
Uplink Frequency - GHz	30			
Min Elevation Angle - degree	18			
Max Slant Range - km	2961.8	1881.6	2961.8	1881.6
Path Loss - dB	191.4	187.4	191.4	187.4
Min EIRP Required - dBW	15.7	11.7	18.7	14.7

3.2.3 Coding Gain

Even with our antenna's high gain, those EIRP values were improper for designing a small sensor. The solution was to spread the signal by a PN sequence or

Barker code. That gave two advantages: more secure link and additional dBs in the link budget and so reduced the minimum transmitted power. Spreading or coding gain for any code can be expressed by:

$$Coding\ Gain\ (dB) = 10Log_{10}\left(\frac{ChipRate}{BitRate}\right) \tag{11}$$

Spreading gave two disadvantages as well: increased bandwidth of the transmission and more complexity of the system. The block diagram in Fig 3.2 shows the added hardware in our transmitter and receiver to attain this goal. At the transmitter side, the message is multiplied by a high bit (*chip*) rate sequence. The result will be a stream of *chips*. This stream then modulates the RF carrier and is transmitted with the same power as the message signal. The word 'Spreading' here comes from spreading the RF energy over a wide bandwidth.

In the receiver, the received chips signal is multiplied by a stored sequence and the result is integrated coherently. If the right sequence is present in signal, the integrator will have a finite output; otherwise the integrator output will be almost zero.

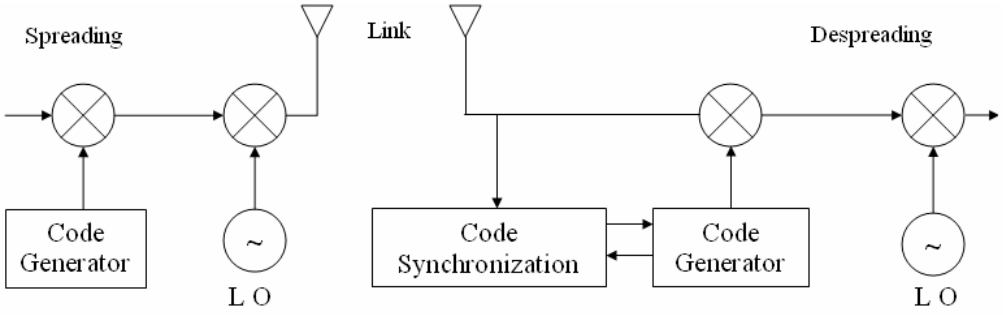

Figure 3.2: Spreading and despreading hardware implementation

In our simulation using ADS, the available code was PN code with 2^{15}-1 bits M-sequence.

Correlation was done by applying the same PN-sequence generator output delayed by the elapsed time the message needs to go from the output of the transmitter modulator to the input of the receiver correlator. The exact delay can be measured by either adding up the delays in each component between the two ends or by simply

specifying the start and the ending points for the simulation and then it will be done automatically.

3.3 Antenna

3.3.1 Gain and Beamwidth

Two parameters were investigated in the antenna part: the gain which controls the transmitted power and the beamwidth which controls the scanning process. Our parametric study showed that a transmitted power in the range of mill watts was enough to deliver enough carrier power to the satellite receiver to get a BER of less than 10^{-5}. This result was based on using a high gain antenna. A phased array antenna with gain up to 20.9 dB was used to transmit the power. Several cases were studied. Three dimensions were considered, 2.35, 3.35 and 7 cm. The simulation ARRAY showed that the larger aperture gives the higher gain and the narrower beamwidth. The two first cases, 2.35 and 3.35 cm diameter antennas used the Ka band frequency while the larger one, the 7cm, used the L band.

3.3.2 Material and Fabrication

The antennas used circular patch elements with hexagonal sequence for low side lobes. Duroid substrate was used as it is characterized by a high dielectric constant (epsilon), stability of properties with frequency in the range GHz, small loss angle, and ease of machining. Next chapter discusses the design procedure of each case.

3.3.3 MEMS Phase Shifters

Microwave phase shifters are essential components in phased array antennas. Phase shifters are used to change the transmission phase angle of a network. MEMS technology is a key innovation for building low-loss phase shifters and other control circuits at millimeter-wave frequencies. Traditional electronic phase shifters are generally built on GaAs and use MESFET's [15] or pHEMT's as switches.

Phase shifters can be analog or digital. Analog phase shifters are built using varactor diodes and provide a continuously variable phase from 0 to 360°, perhaps controlled by a voltage. Digital phase shifters are usually built using switches and provide

a discrete set of phase states that are controlled by two-state "phase bits." The highest order bit is 180 degrees, the next highest is 90 degrees, then 45 degrees, etc, as 360 degrees is divided into smaller and smaller binary steps.

Most phase shifters are of the digital variety, as they are more immune to noise on their voltage control lines. The scanning resolution and sidelobes levels are directly related to the number of bits used. For example, a three bit phase shifter would have a 45 degree least significant bit (LSB) and can provide phase shifts of 0, 45, 90, 135, 180, 225, 270 and 315°. A four bit phase shifter can provide better resolution with 22.5° steps phase shifts of 0, 22.5, 45, 67.5, 90, 112.5,135, 157.5, 180, 202.5, 225, 247.5, 270, 292.5, 315 and 337.5°.

Most systems require a 3-bit or a 4-bit design, except for some high-performance systems that may require 5- or 6-bit phase shifters [16]. In this project, a 3-bit phase shifter was tested and showed an error of few degrees. A 4-bit phased shifter was then tried and showed negligible errors (less than 2°). However, for our application both phase shifters can be used. More bits-phase shifter wouldn’t be a good choice for low cost system.

In ADS, the phase shifter is replaced by an attenuator in the circuit. The phase shift is accounted for in the ARRAY software. According to [17] and [18], the average insertion loss for fabricated 4-bit phase shifters is between 1.5 and 2.25 dB. An attenuator with 2 dB was inserted before the antenna component in the ADS design. Figure 3.3 shows a typical 4-bit phase shifter using switch delay lines and series micromachined switches.

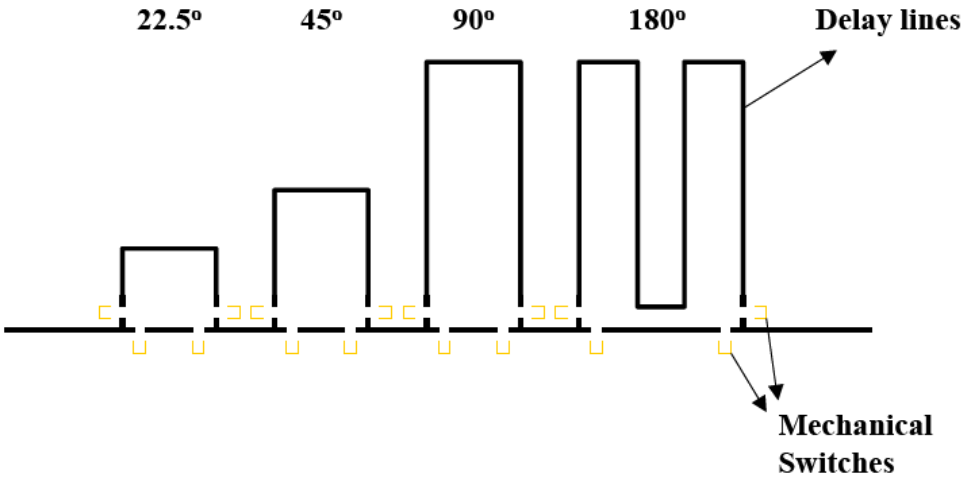

Figure 3.3: 4-bit true-time phase shifter architecture based on switched delay lines and series micromachined switches

The detailed design of the antenna is discussed in the next chapter. The scanning process for the two phased arrays is illustrated in 2 and 3D figures.

Chapter 4

Antenna Design

Chapter 4 talks about the detailed design of the proposed antennas. First, the two phased array antenna designs are discussed, followed by the figures of the main beam for each. Second, the antenna beam scanning process in 2-D and 3-D is shown in figures and explained in the discussion. Third, comparison among the three antennas and comparison between literature values and our simulation results is provided. Finally, the chapter briefly discusses the fabrication process for printing these antennas and the material used for that as well as the feeding details for the elements used.

4.1 Introduction

Our parametric study showed that transmitted power in the range of mill watts was enough to deliver enough carrier power to the satellite receiver to get a BER of less than 10^{-5}. This result was based on using a high gain antenna. A phased array antenna with gain up to 20.9 dB was used to transmit the power. Many cases were studied. Three dimensions were considered, 2.35, 3.35 and 7 cm. Larger aperture relative to wavelength gives the higher gain and the narrower beamwidth. The two first cases, 2.35 and 3.35 cm diameter antennas used the Ka band frequency while the larger one, the 7 cm, used the L band. The following are the detailed design steps for each case:

4.2 19-Element Antenna

4.2.1 Design and Performance

This is the smallest designed antenna in our project. It operates at the Ka band at frequency of 30 GHz. As shown in Fig 4.1, it consists of 19 circular microstrip patch elements with 0.175 λ radius and hexagonal sequence. The elements are half-wave length spaced to avoid any grating lobes and so the diameter was 4.7 half-wave lengths or 2.35 cm. In order to get the highest gain possible, the amplitude distribution is uniform.

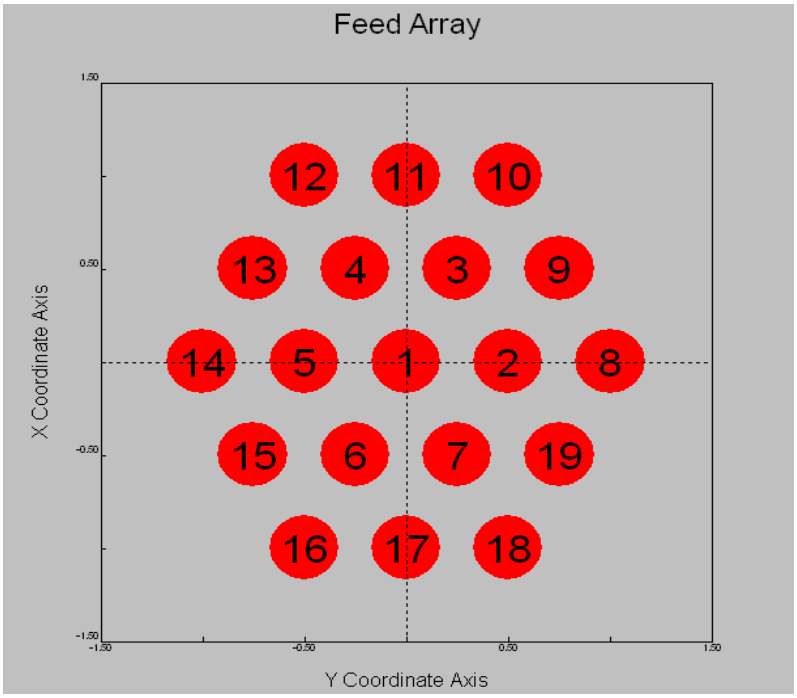

Figure 4.1: Snapshot of the 19-element hexagonal array as seen on software

4.2.2 Scanning Process

The designed antenna covers the space above 13 degree above horizon. The scanning process starts by the main beam looking vertically in zenith (θ = 0°, φ = 0°) which is shown in Figure 4.3, transmitting for a period of time equal to the dwell time at that angle, then shift the beam down in theta by a value equal to the 3-dB beamwidth of the (θ = 0°, φ = 0°) beam. Figure 4.4 shows the second step of the scanning process. The main beam is directed to the point (θ = 22.1°, φ = 0°) which is at the edge point of the 3-dB beamwidth of the first step in Figure 4.3. The antenna will stop at this step again for a certain dwell time, transmits and then starts to move around the vertical axes in steps equal to the angle φ 3-dB beamwidth of the second beam and so on, until all the space above an angle of 13 degrees is covered by the different antenna beams. The last stage in θ will be at 66.3°. This stage, as shown in Figure 4.6, has the narrowest beamwidth in φ angle and so required the largest number of steps around the vertical axes to cover the 360° space. The total number of steps needed was found to be 34 steps. Figure 4.2 shows

the scanning steps in θ. The figure shows the first step at 0° which has the narrowest beam. The following beams become wider and wider as theta increases.

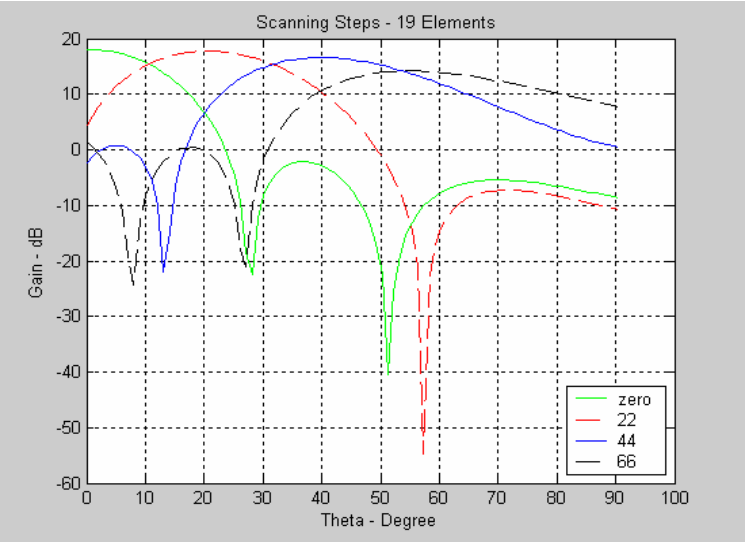

Figure 4.2: 19-element antenna scanning steps in θ

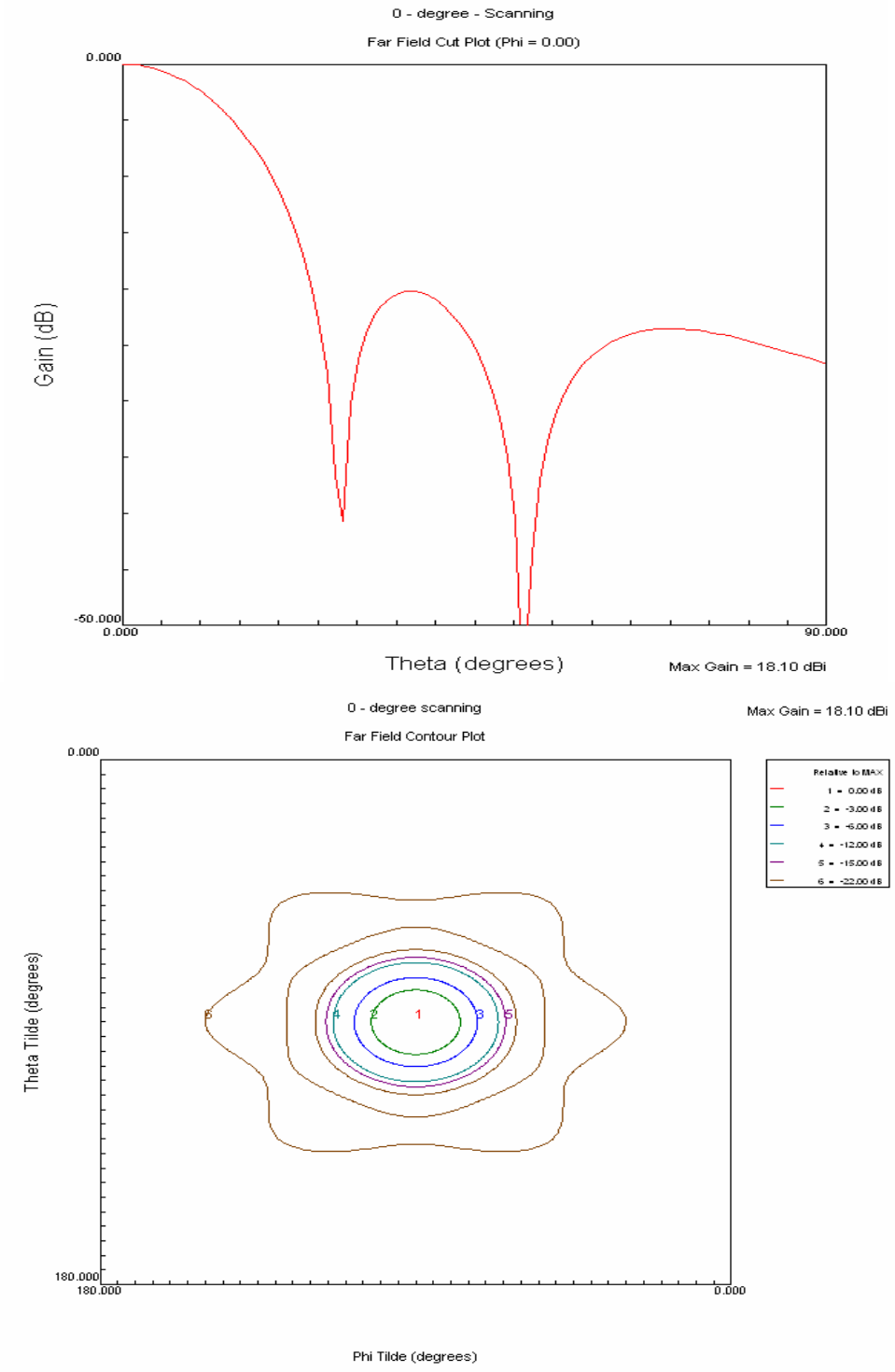

Figure 4.3: Broadside pattern and contour plot for the 19-element array: The gain of the planar array is 18.10 dBi and the first (and highest) SLL is -20.3 dB relative to the peak.

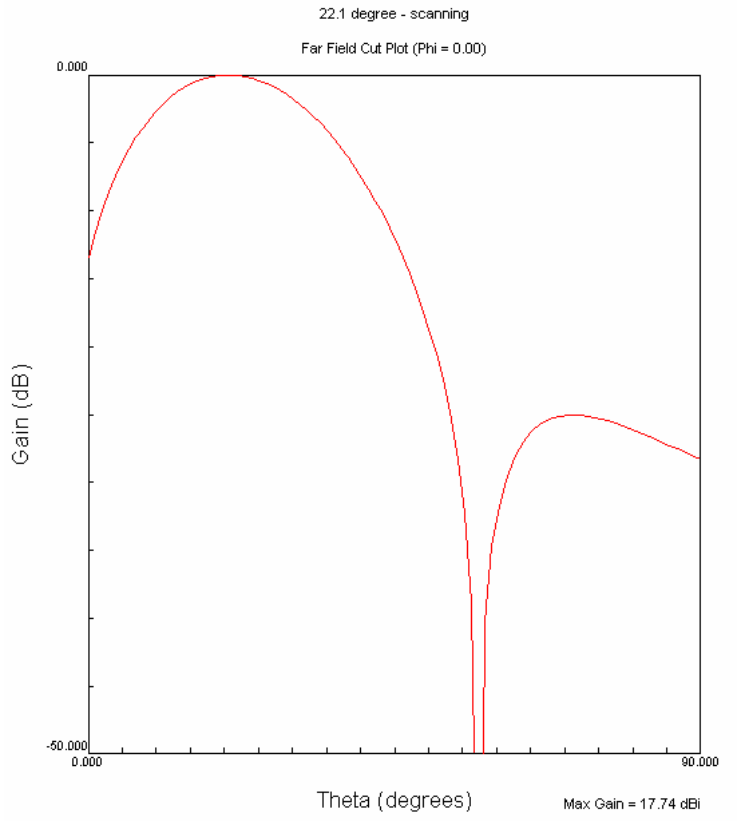

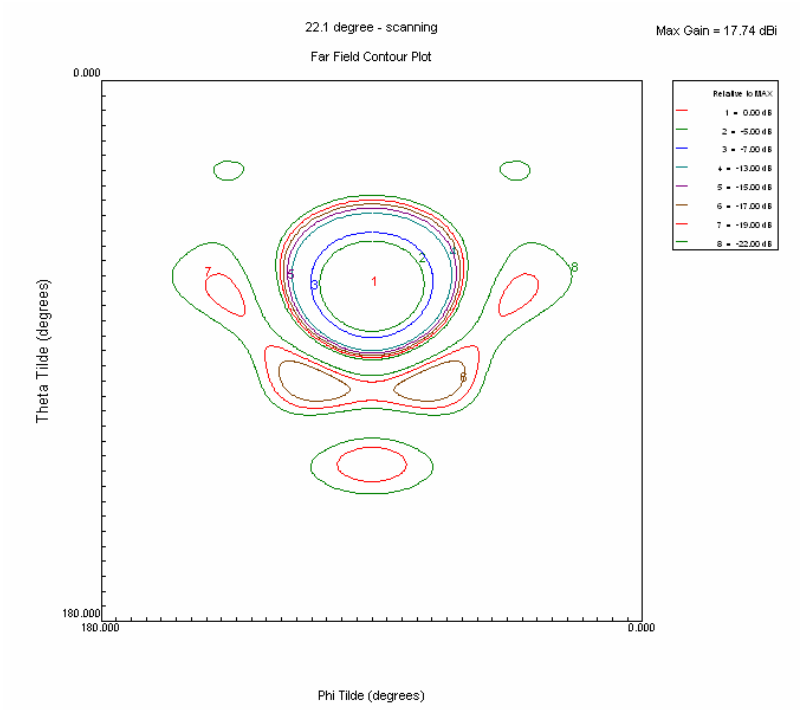

Figure 4.4: 22.1° scan pattern and contour plot for the 19-element array

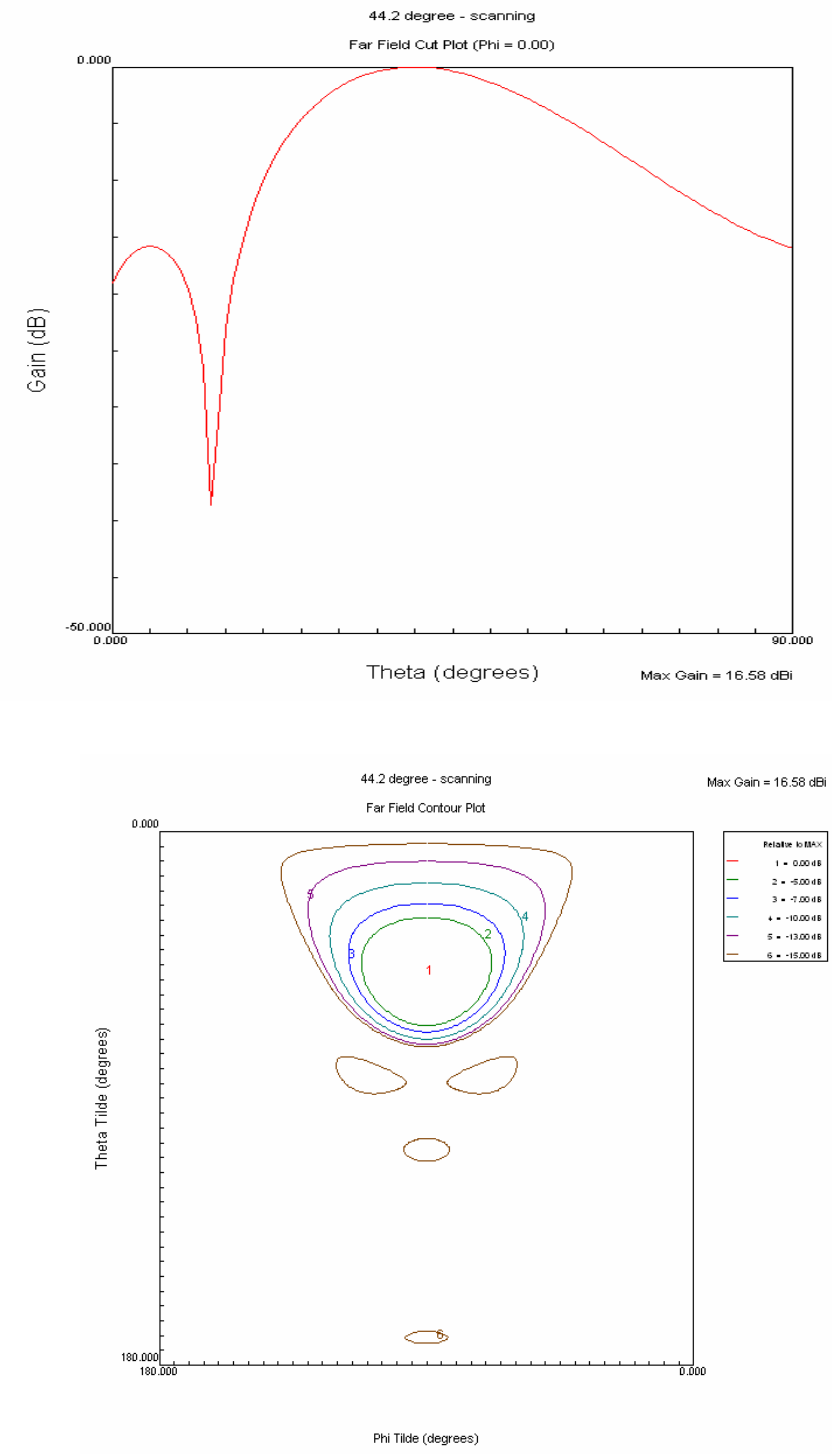

Figure 4.5: 44.2° scan pattern and contour plot for the 19-element array

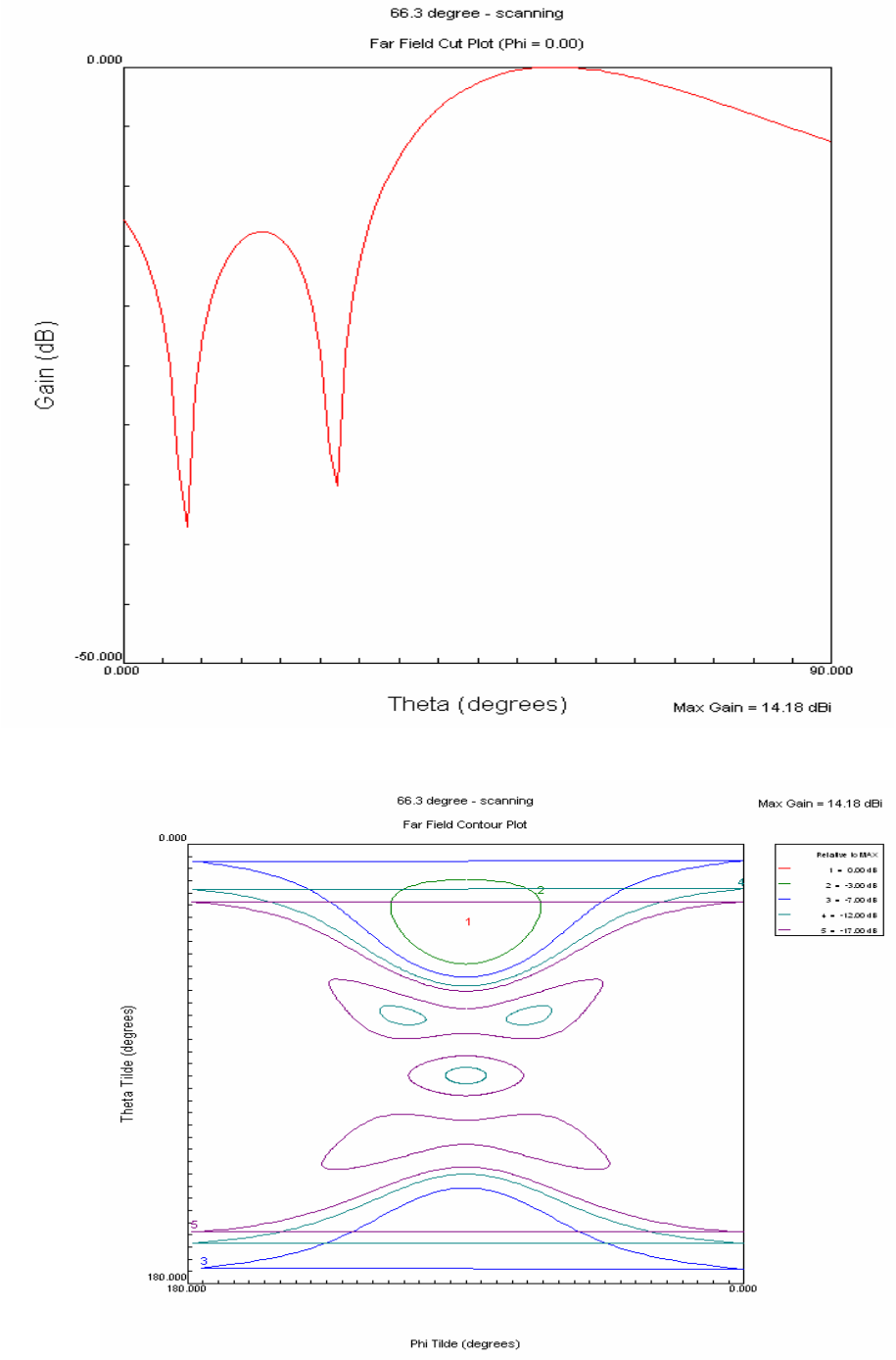

Figure 4.6: 66.3° scan pattern and contour plot for the 19-element array

The designed antenna will be printed on the top of the sensor package facing up. The total area of the 2.35 cm case is 4 half-wave lengths plus 2 patch radiuses which is equal to 2.35 λ or 2.35 cm. This antenna was found to be smaller in area than the American quarter (25 cents).

4.3 37-Element Antenna

4.3.1 Design and Performance

The 37-elemet antenna is similar to the 19-element antenna in every thing except the number of elements, total size, and performance. It operates at the same Ka band and the same frequency, 30 GHz but with 37-elements instead of 19 as shown in Fig 4.7.

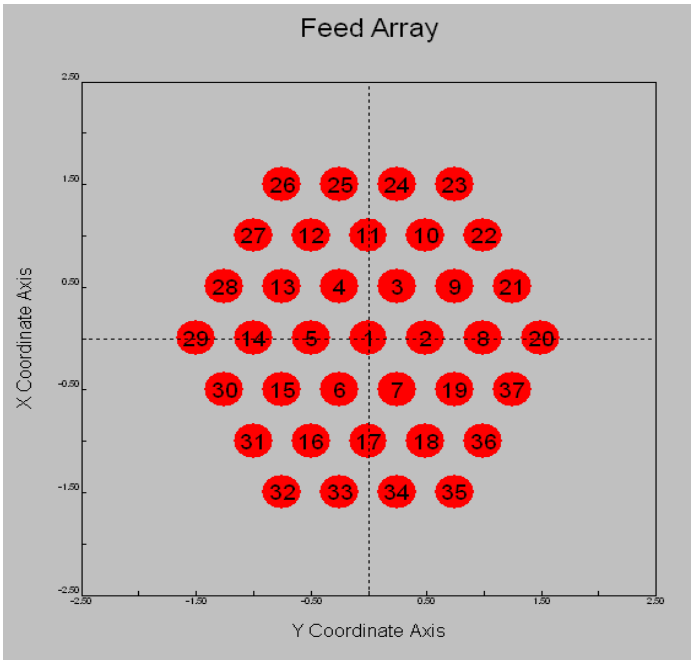

Figure 4.7: Snapshot of the 37-element hexagonal array as seen on software

The array diameter is 3.35 λ or 3.35 cm. The resultant maximum gain was improved by more than 3 dB. The beamwidth of the array at all stages is narrower, so 18 more scanning steps were needed to cover the same space. From a fabrication point of view, this would require more complicated memory or circuitry and as a result larger package.

To compensate for the 3 dB loss, resulting from reducing the antenna size, in the antenna gain, many choices are available: doubling the transmitted power, using longer code sequence to double the coding gain or restricting the application to shorter links i.e. (LEO 780 km instead of LEO 1410 km). The first choice would be more preferred since some space for a larger battery/solar cell was already added by increasing the antenna size.

4.3.2 Scanning Process

The scanning process is the same as in the 19-element antenna case but with more steps and less dwell time at each step since larger antennas give narrower beams. Figure 4.8 shows the scanning steps in θ. More scanning steps were needed and the beams were narrower but with higher gain. The detailed scan pattern and contour plot for each step in θ are shown in Figures 4.9 - 4.13.

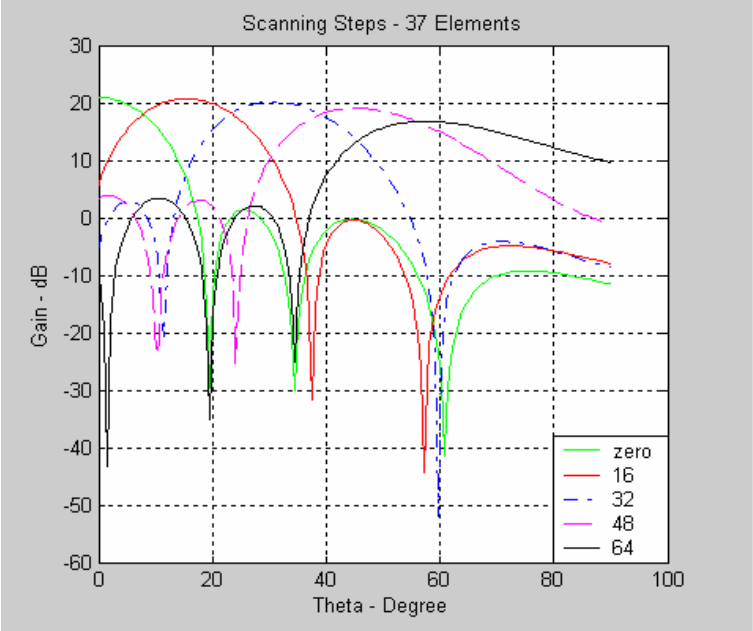

Figure 4.8: 19-element antenna scanning steps in θ

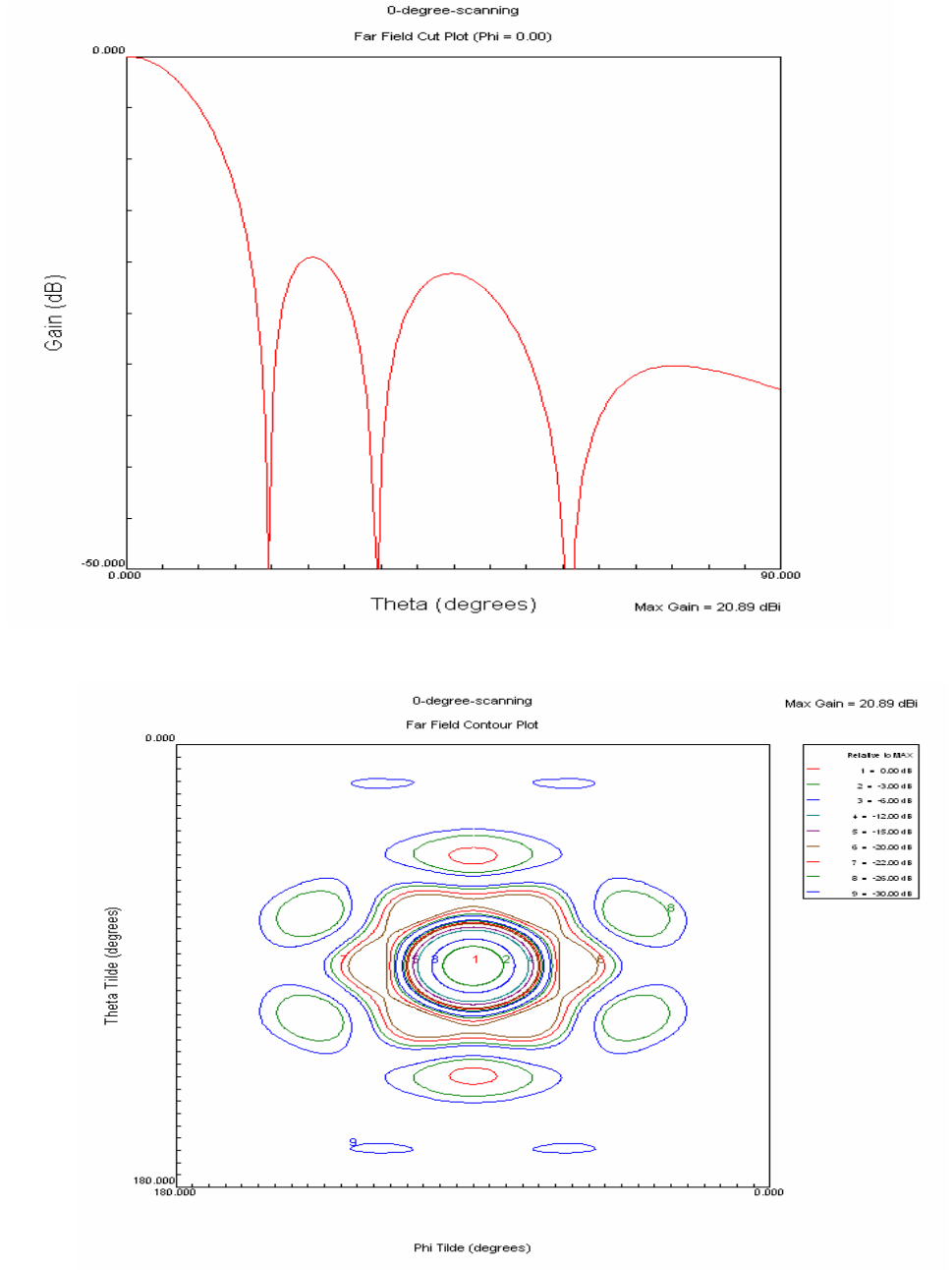

Figure 4.9: Broadside pattern and contour plot for the 37-element array: The gain of the planar array is 20.89 dBi and the first (and highest) SLL is -19.8 dB relative to the peak

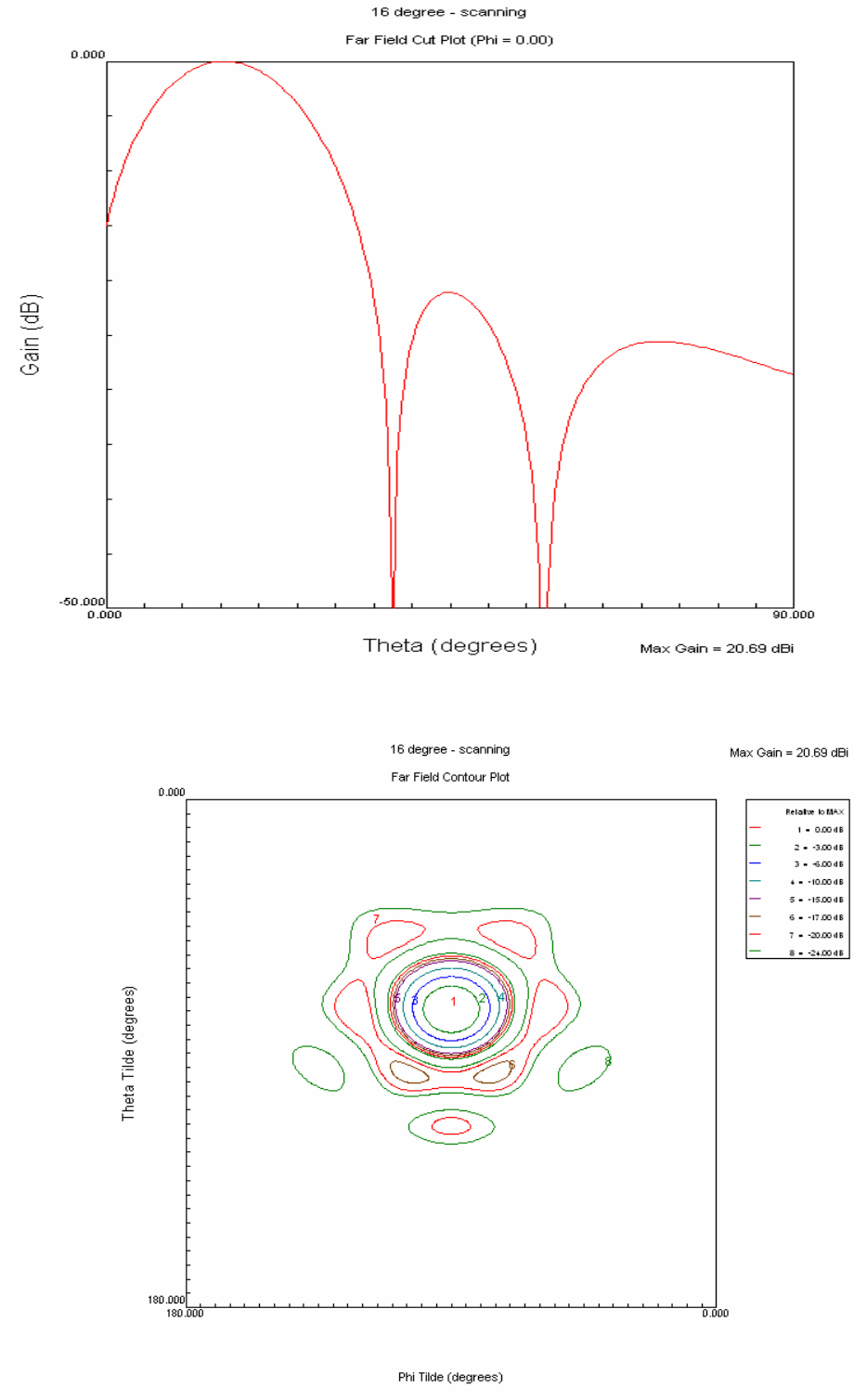

Figure 4.10: 16° scan pattern and contour plot for the 37-element array

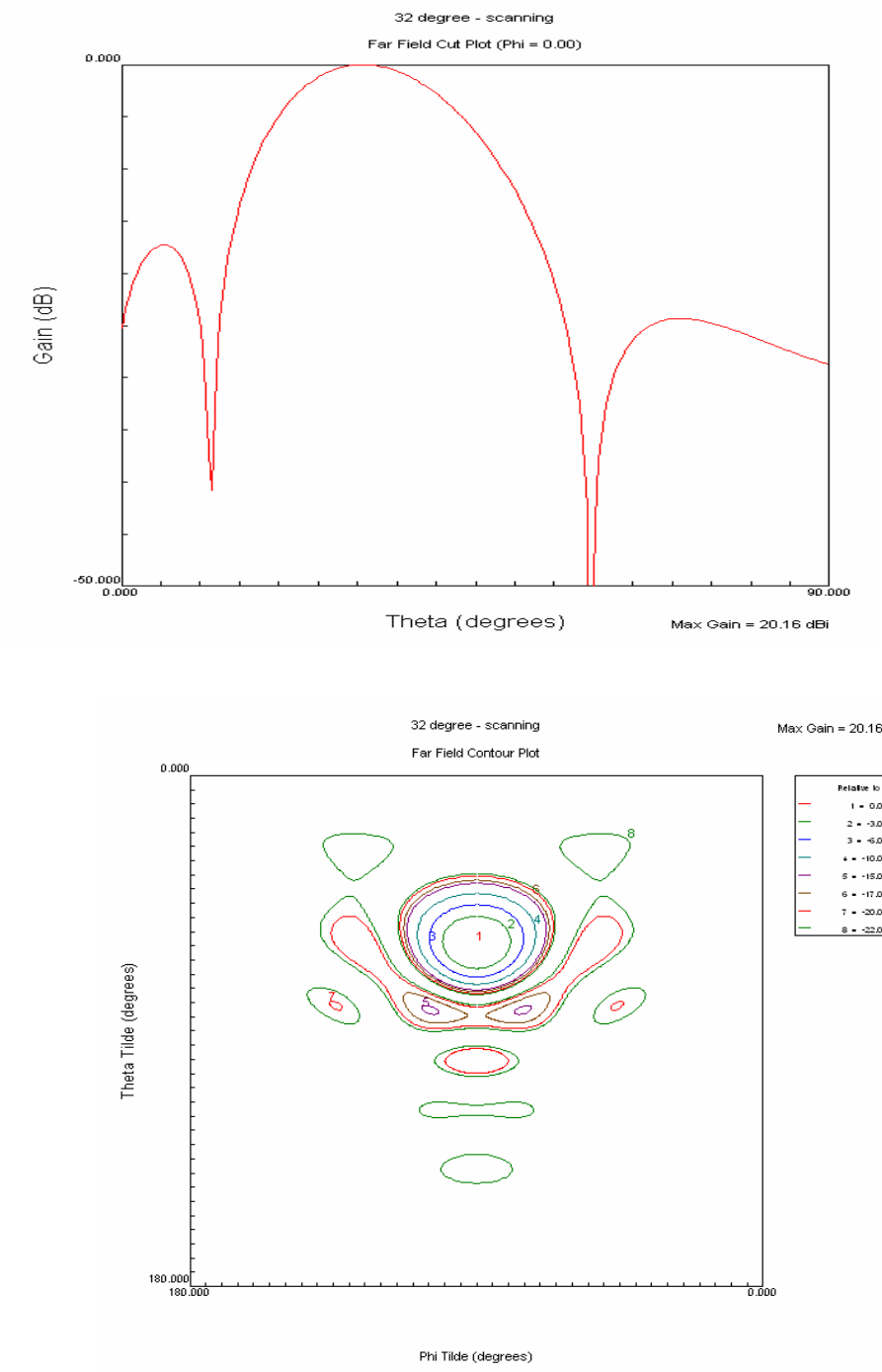

Figure 4.11: 32° scan pattern and contour plot for the 37-element array

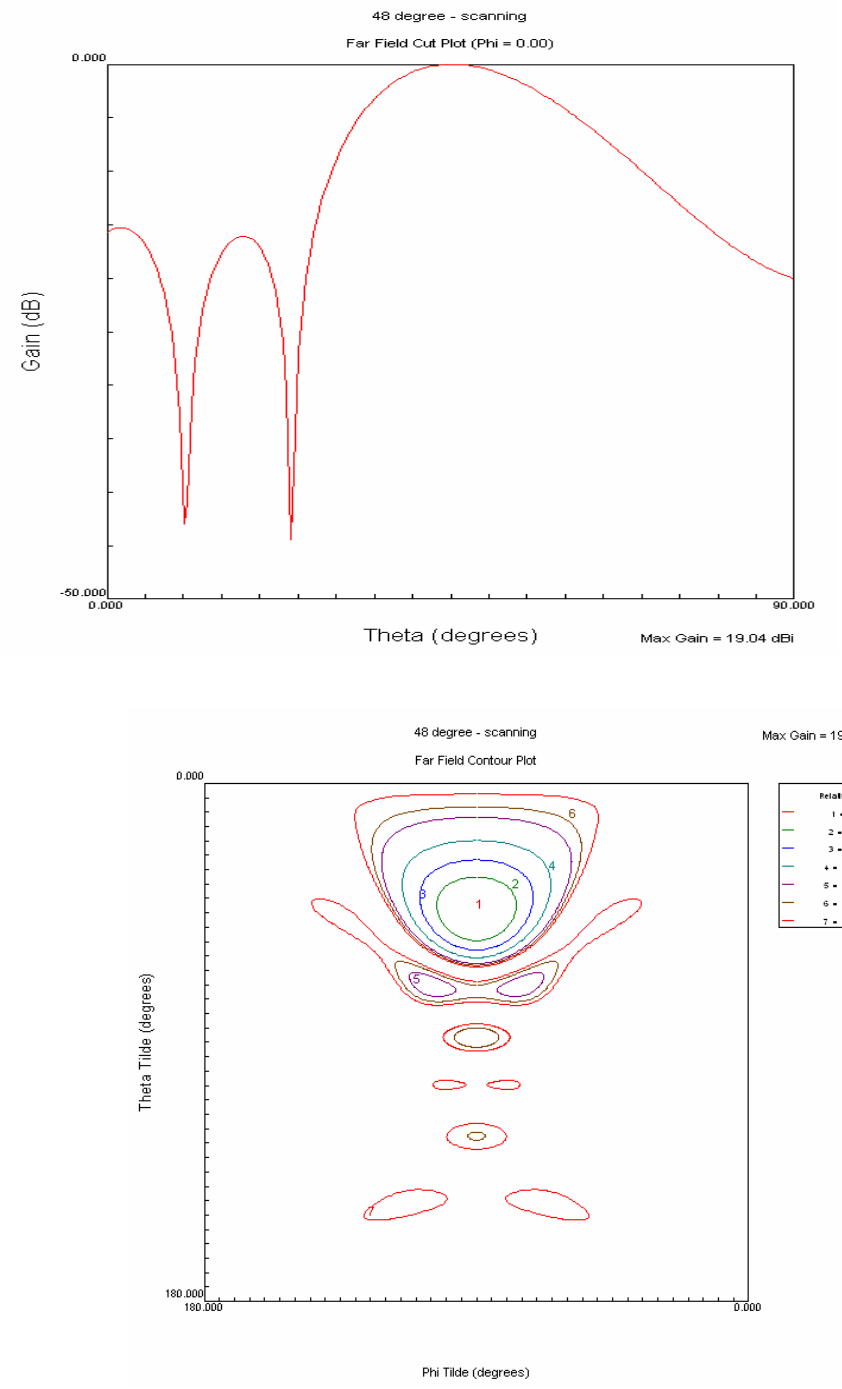

Figure 4.12: 48° scan pattern and contour plot for the 37-element array

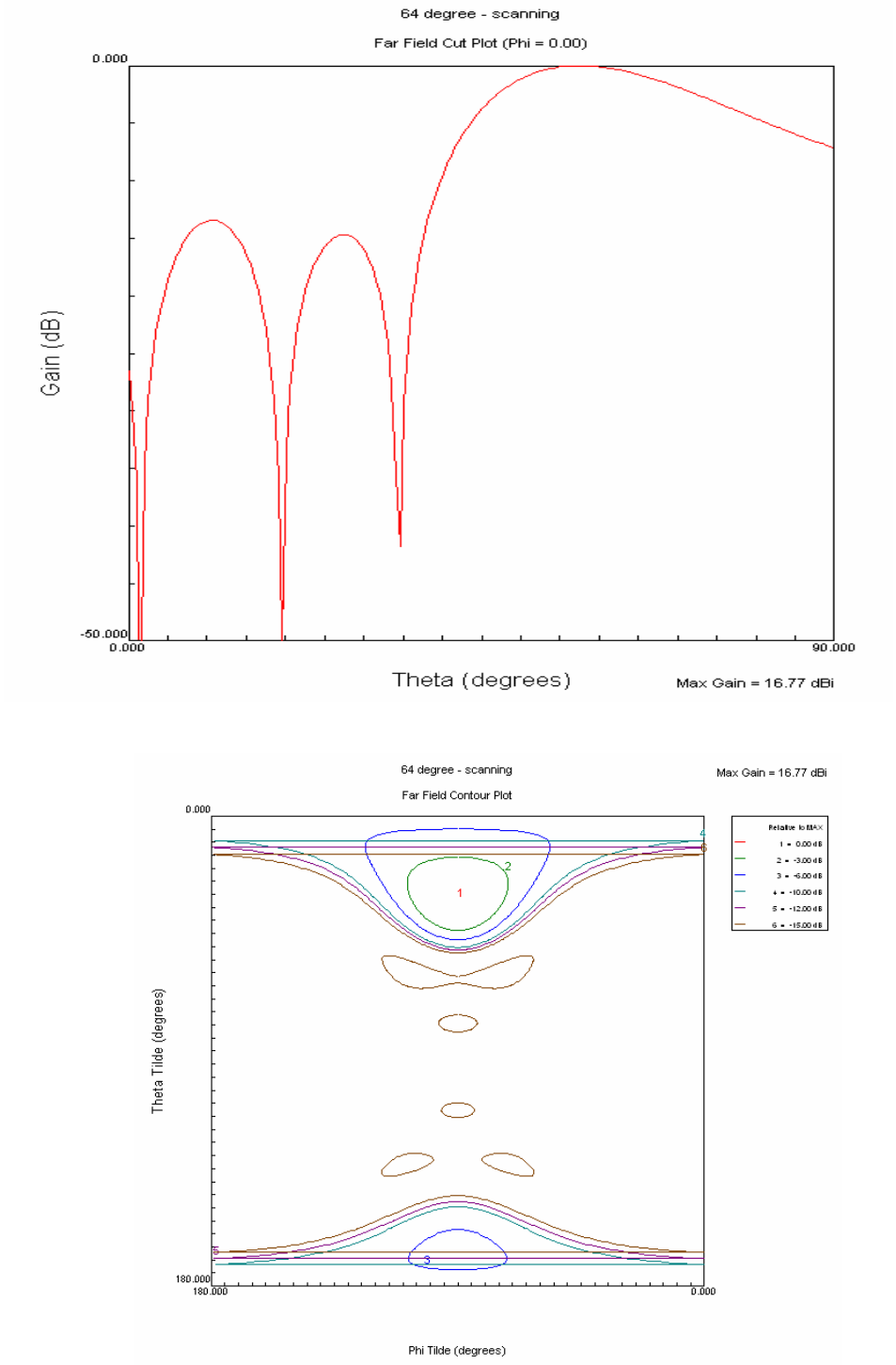

Figure 4.13: 64° scan pattern and contour plot for the 37-element array

4.4 Dwell Time

Figure 4.14 shows the relation between the dwell time and the antenna beamwidth for LEO satellite links of 780 and 1400 km. It is clear that the wider the beamwidth the longer time the antenna 'sees' the satellite. On the other hand, the wider beam means less gain, and as a result, less received power.

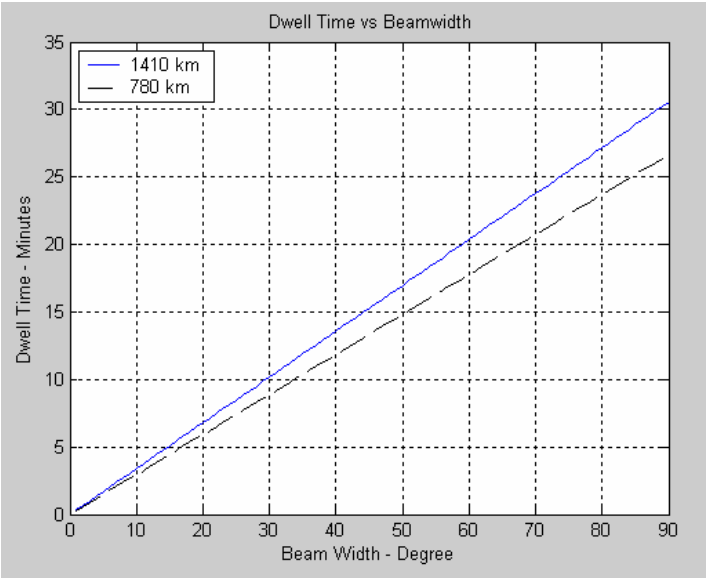

Figure 4.14: Beamwidth vs. Dwell Time

As shown, links with higher altitude show longer dwell time because of two reasons: the satellite in higher altitudes needs longer time to pass the circular distance at certain angle, and the higher orbit is the slower it will be, because gravity will be weaker.

4.5 3D Scanning

The scanning processes for both antennas, the 3.35 cm antenna and the 2.35 cm, follow the same procedure. The 3.35 cm antenna is larger and so it has higher gain at each angle and as a result smaller beamwidth. The smaller beamwidth requires more steps in the scanning process to cover the same space. The scanning steps for the 2.35 cm and the 3.35 cm antennas are summarized in the Tables 4.1, 4.2 below. The antenna starts transmission at ($\theta = 0°$, $\varphi = 0°$) for the related dwell time, then shifts the beam down in theta by a value equal to the 3-dB beamwidth of the ($\theta = 0°$, $\varphi = 0°$) beam. The antenna

will stop at this step again for a while, transmits and then starts to move around the vertical axes in steps equal to the 3-dB beamwidth of the second beam and then goes down again in theta and makes another round and so on until all the space above the minimum angle is covered by the different antenna beams.

Table 4.1: Scanning process details – 19-element antenna case

Theta θ °	Gain dB	θ 3dB BW°	φ 3-dB BW°	Φ steps	Step - degree
0	18.1	22.1	22.1	1	360
22.1	17.75	24	68.19	6	60
44.2	16.58	28	36.1	10	36
66.3	14.18	35	22.06	17	21.18
				34	

As shown in the two tables, while the 2.35 cm antenna will have to make a total of 34 steps only to cover all the space above the angle of 13°, the 3.35 cm antenna will have to make a total of 53 steps to cover all the space above the angle of 18°. The two values, 13° and 18° came from the fact that the real last point in the coverage will be at 3-dB down from the last angle of scanning.

Table 4.2: Scanning process details – 37-element antenna case

Theta θ °	Gain dB	θ 3dB BW°	φ 3-dB BW°	Φ steps	Step - degree
0	20.89	16	16	1	360
16	20.69	17	65	6	60
32	20.16	18.3	34.6	11	32.73
48	19.04	22	24	15	24
64	16.77	26	18.6	20	18
				53	

Figure 4.15 shows the 3.35 cm antenna scanning process using fake beams. The faded colors represent the previous case of the beam and the regular colors represent the recent case in the frame. First frame shows the beam at (θ = 0°, φ = 0°) which will be the tallest as it has the highest gain. Next frame shows the original beam in transparent colors and the second beam when scanned down in theta to θ = 22.1°. This beam is shorter than the first one because it has less gain, and wider because the beamwidth is higher. The

antenna in frame # 3 starts to shift the beam in the angle φ in equal steps for 60° until it makes a full round and goes back to the starting point as shown in frame # 4 (which is the same point in the second figure). In frame # 5, the second down shift in theta occurs. As listed in Table 4.2, the next value of theta will be 44.2° from the vertical axes or 45.8° from horizon. The antenna again will scan in φ in frame # 6 and finish the round in frame # 7 to make the last down shift in θ and so on until it covers the required space in 53 steps and goes back again to the starting point in frame # 12.

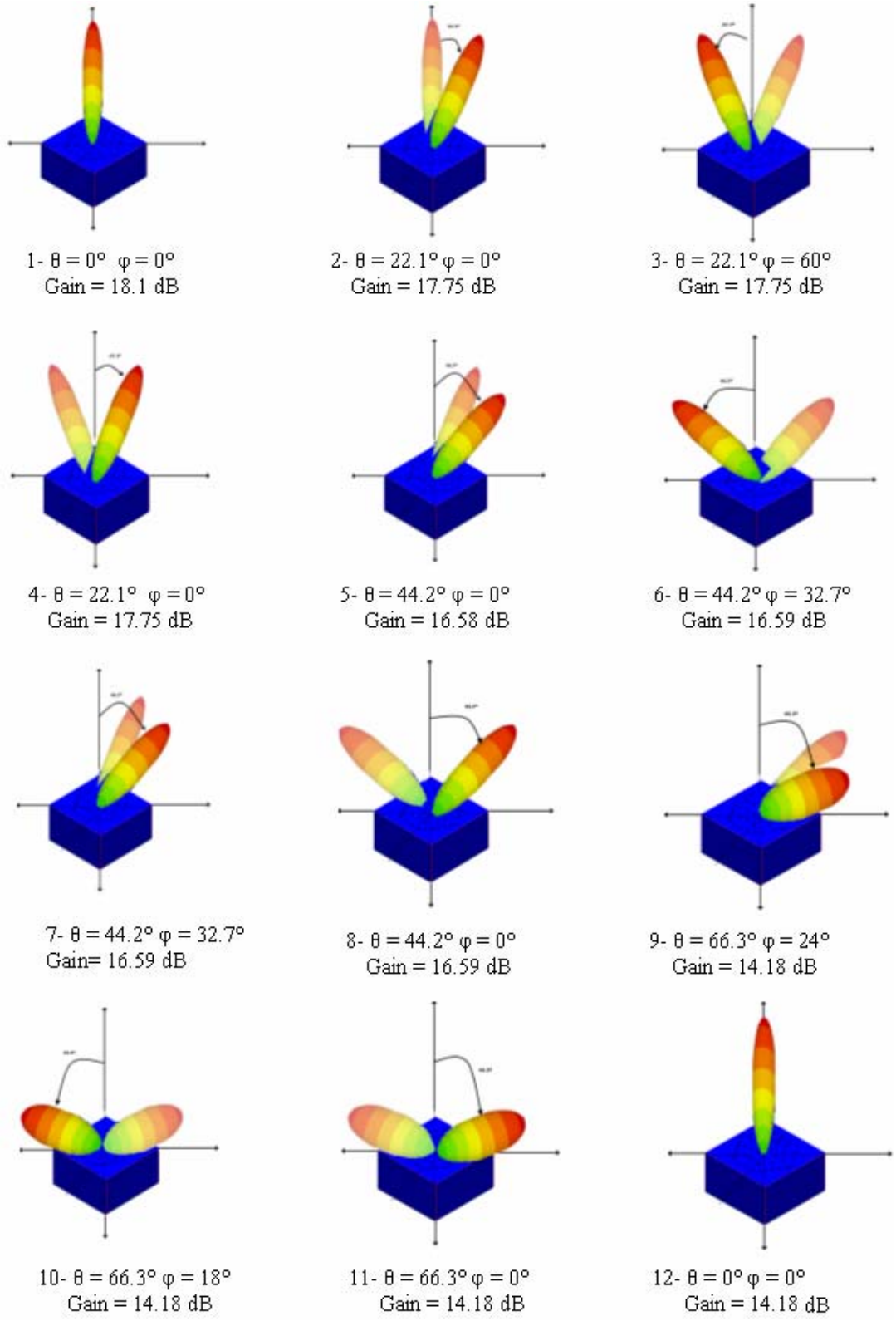

Figure 4.15: 3D beam scanning – 37-element antenna

4.6 Cosine Law

Planar antennas with isotropic elements theoretically lose a gain magnitude of 10 $\log_{10}$ cos (θ) when the mean beam is scanned to an angle θ from the vertical axis. So it reaches the maximum gain at θ = 0° and reaches the minimum at θ = 90° or parallel to the horizon. Figure 4.16 shows the gain reduction with increasing the angle θ for both the Cosine law and the software used ARRAY for the 3.35 cm antenna case. One can see that the simulation gives almost the same results given theoretically up to θ = 45°. After that, the deviation starts to increase slightly until it reaches a maximum of 0.4 dB at θ = 60° then starts to decrease again. The small difference between the two curves resulted from using circular patch elements instead of the isotropic elements which do not exist in reality. Using the circular patch elements which give a different pattern from the isotropic elements pattern changes the reduction factor according to their pattern.

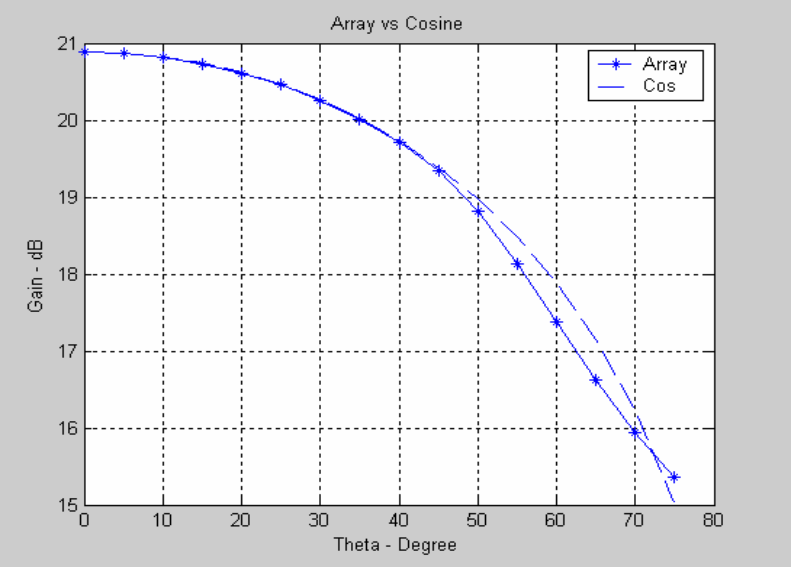

Figure 4.16: Scan gain reduction, theoretical and simulation results

4.7 Single Element Antenna

As the L band is considered a common communication band for many satellite operators like Iridium, Globalstar and Orbocomm, it was necessary to study the possibility of designing an antenna with feasible size and acceptable gain at this band. As

in all low frequency antennas, the first problem antenna engineers always face is the size. At frequency of 1.5 GHz, the wavelength is 20 cm which is considered very large size for this application. In this case, the phased array idea was difficult to be applied, especially with the long wavelength. Instead, the phased array was replaced by a single circular patch element that covers large space but with less gain. The radius of this element in Figure 4.17 was 0.175 λ or 3.5 cm at 1.5 GHz which gives the patch element a total area of 38.48 cm². The 3-dB beamwidth was 90° so there was no need for scanning process. This would also simplify the circuits and save some power by reducing the number of RF components used.

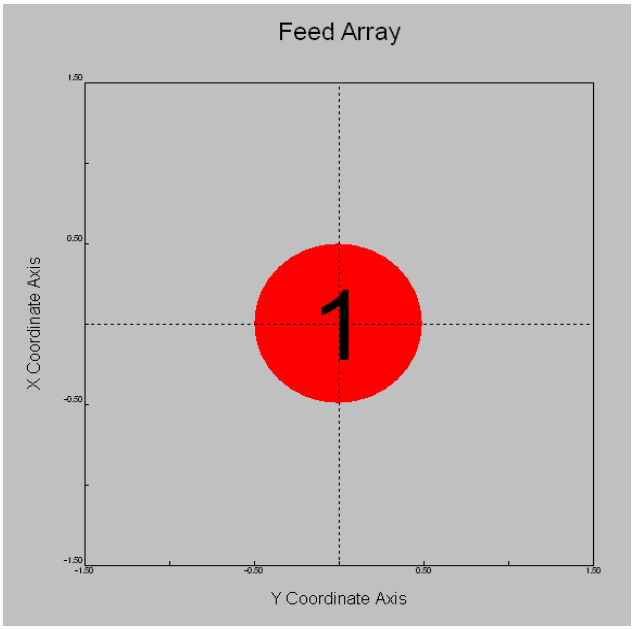

Figure 4.17: Snapshot of the single-element antenna as seen on software

As shown in Figure 4.18, the total gain for the one element is 6.8 dB. If one wants to compare this value to the Ka band antennas, one sees that its gain is 14 dB less than the 37-element antenna and 11.3 dB less than the 19-element one at the Ka band. But since the path loss calculated by (10) is less by 26 dB at the L band than the Ka band, the single element antenna required less power from the transmitter and smaller battery.

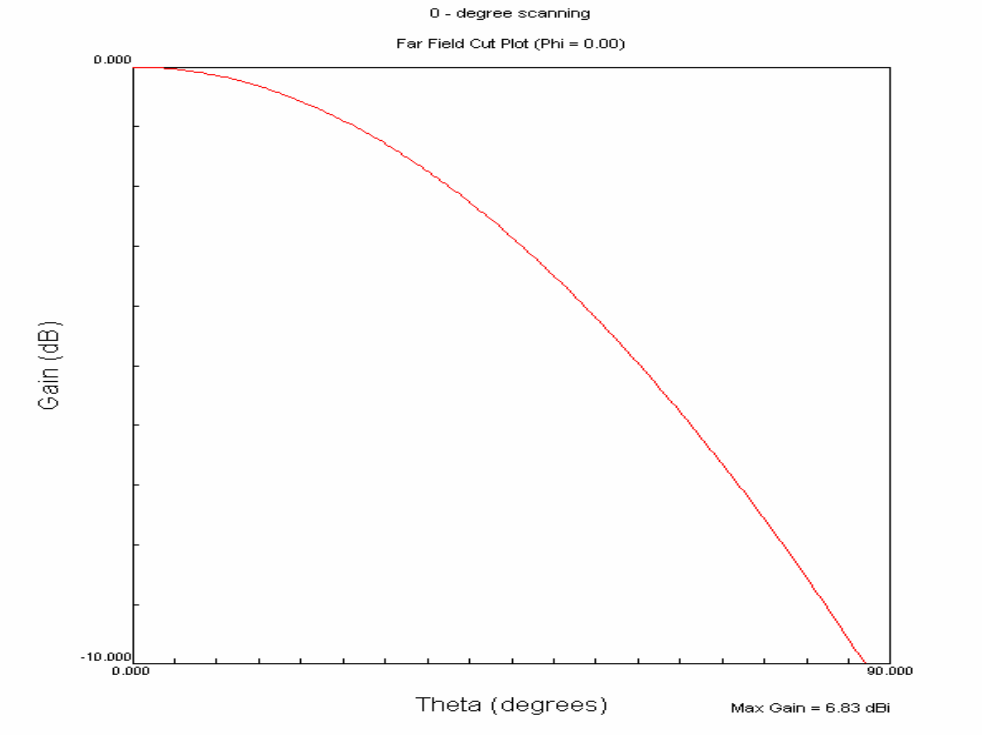

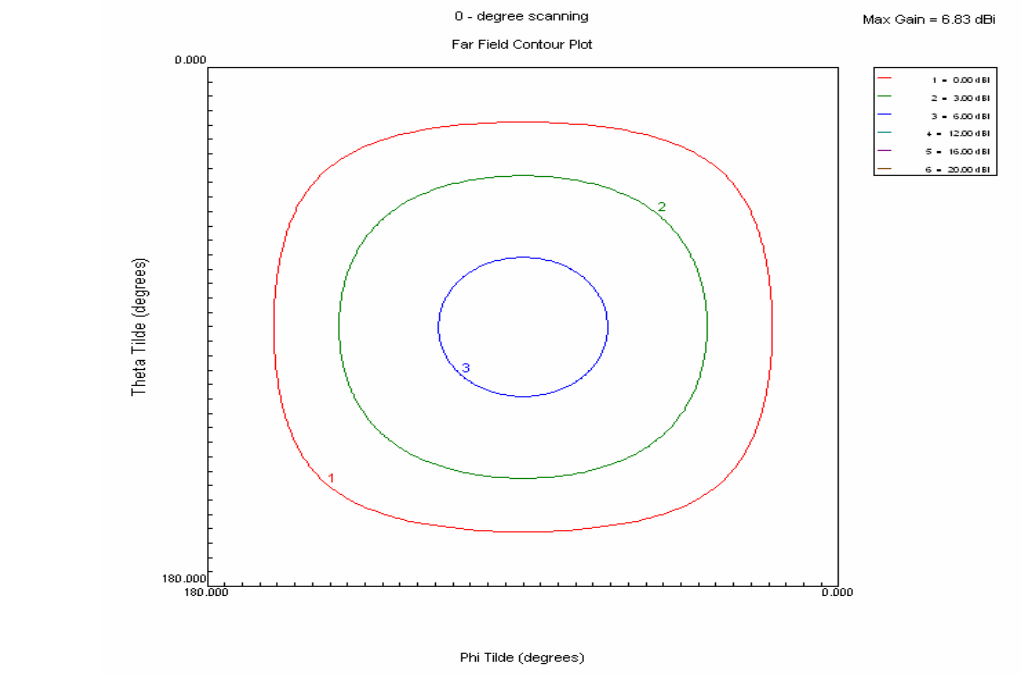

Figure 4.18: Broadside pattern and contour plot for the single-element: The gain of the circular patch is 6.83 dBi

4.8 Comparison of Three Antennas Designs

Three antenna models were studied in this chapter; two work at Ka band and one at L band. The Ka band antennas are smaller in size than the L band antenna. The gain were higher for the two Ka band than the one at L band, this is due to two reasons: the more number of elements used, and the higher frequency. An approximate formula for the planar antenna gain can be found in [4].

$$Gain = \frac{4\pi.\rho.A}{\lambda^2} \tag{12}$$

where ρ is the aperture efficiency, A is the physical area of the aperture and λ is the wavelength.

The L band antenna has some advantages as well. No scanning is required because of the wide beamwidth and the path loss is less. The beamwidth in the Ka band antennas is narrow and requires the antenna to keep searching the space for the satellite. Scanning requires changing of the phases. Less scanning steps means less phase changes and less complexity in the memory unit. The number of scanning steps is directly related to the beamwidth of the main beam. Many formulas that relate the gain to the beamwidth can be found in the literature. One of the most used formulas is:

$$Gain = \frac{33000}{\theta^\circ \phi^\circ} \tag{13}$$

Note that the gain in formulas (12) and (13) is in ratio.
Table 4.3 summarizes the specifications of the three designed antennas.

Table 4.3: Performance summery

Antenna	Frequency	Diameter	Max Gain	Coverage	Scan Steps
19-elemenet	30 GHz	2.35 cm	18.1 dB	θ > 12.7°	34 Step
37-element	30 GHz	3.35 cm	20.8 dB	θ > 18°	53 Step
Single-element	1.5 GHz	7 cm	6.8 dB	θ > 45°	No scanning

4.9 Comments on the Fabrication

Building the proposed antennas should be an easy process using circuit printing techniques. 3- or 4-bits phase shifters can be built using MEMS. Both cases were studied and the results in Tables 4.4, 4.5 show that in both antenna cases, the error in degrees and dBs is considered negligible. According to the first two columns in both tables, the maximum gain reduction in dBs was 0.4 and the main beam direction error didn't exceed 3 degrees for both phase shifters. Last column shows that the maximum beamwidth error was 2 degrees, so no change in the scanning steps was needed for any of the phase shifters.

In general, the 4-bit phase shifter showed less quantization errors as its resolution is twice the 3-bit one, but it will cost more and require more control circuitry.

Table 4.4: 3-bit & 4-bit phase shifters quantization error – 19-element antenna

Scan Angle θ°	Gain Error - dB		Direction Error °		Beamwidth Error °	
	3-bit	4-bit	3-bit	4-bit	3-bit	4-bit
0	0	0	0	0	0	0
22.1	- 0.2	0	0	0	0	0
44.2	- 0.4	- 0.1	3	0	1	0
66.3	- 0.1	- 0.1	0.2	0.2	1	1

Table 4.5: 3-bit & 4-bit phase shifters quantization error – 37-element antenna

Scan Angle θ°	Gain Error - dB		Direction Error °		Beamwidth Error °	
	3-bit	4-bit	3-bit	4-bit	3-bit	4-bit
0	0	0	0	0	0	0
16	0	0	1.3	0	1	0.5
32	+ 0.1	0	2	0.5	0.3	0
48	- 0.1	0	0.6	0.6	0	0
64	- 0.4	- 0.1	1	0.3	2	2

Figure 4.19 lists all the parameters used in feeding the circular patches and that will be used in fabricating the antennas. All the numbers are in terms of wavelengths. The polarization amplitudes and phases were set to give a right-hand circular polarization.

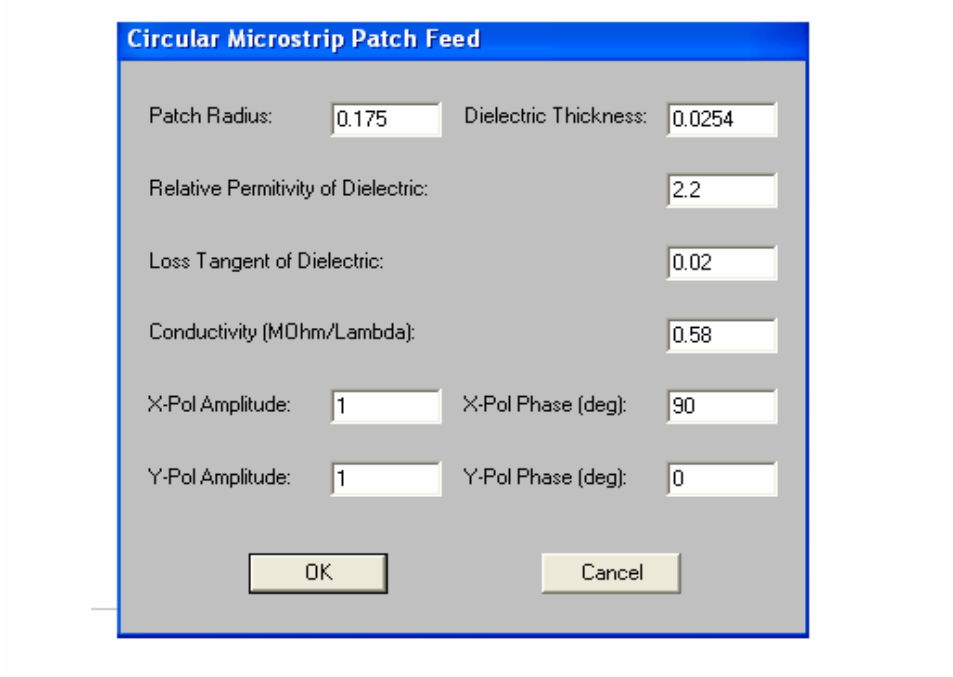

Figure 4.19: Circular patch elements feed details

Upon fabrication, the antenna plane should be facing upward. The assumption made, is that the sensor package will be integrated below the antenna surface. Further assumptions were made and are discussed in chapters 5-7.

Chapter 5

Transmitter-Receiver Simulation and Design Procedure Using ADS

The antenna simulation results from chapter 4 were used in the whole system simulation using ADS software package which is presented in this chapter. Agilent ADS has been used successfully in the simulation of many electrical systems. Examples of work close to the thesis work done using ADS are: using ADS to simulate a transmitter with a single up-converting stage [19]; and designing a radio front-end module at 5 GHz [20]. All currently-available journal articles on Agilent products and applications can be found in [21].

The design in this chapter is discussed for each component for the transmitter and the receiver. The parameters for each component are listed in the figures and discussed through the chapter. This chapter relates theoretical formulas to the values used for each component and explains why every parameter was chosen. The signal is tracked from the (A/D) to the output of the satellite receiver.

5.1 Transmitter

After the completion of the antennas design, all the results from chapter 4 were brought and used in the sensor design. This chapter discusses the design and the simulation of the sensor and the proposed satellite receiver using the ADS simulation package. The whole circuit consists of two main schematics; the time synchronous data flow (TSDF) schematic which includes the digital signal processing (DSP) components, and the Analog RF schematic which includes microwave frequency components. The Agilent *Ptolemy* feature of the ADS enables co-simulation of DSP blocks with the RF and analog simulators within the same schematic [22]. The TSDF enables fast RF simulation, integration with signal processing simulation, and co-simulation with other circuit simulators. Agilent *Ptolemy* helps smoothing the system simulation between different domains.

The two schematics are shown in figures 5.1, 5.2 respectively. They were too large and had many components to be shown clearly in one figure. Instead, the design is

discussed component by component. Each discussion is followed by the sketch of the component with its input and main parameters if needed.

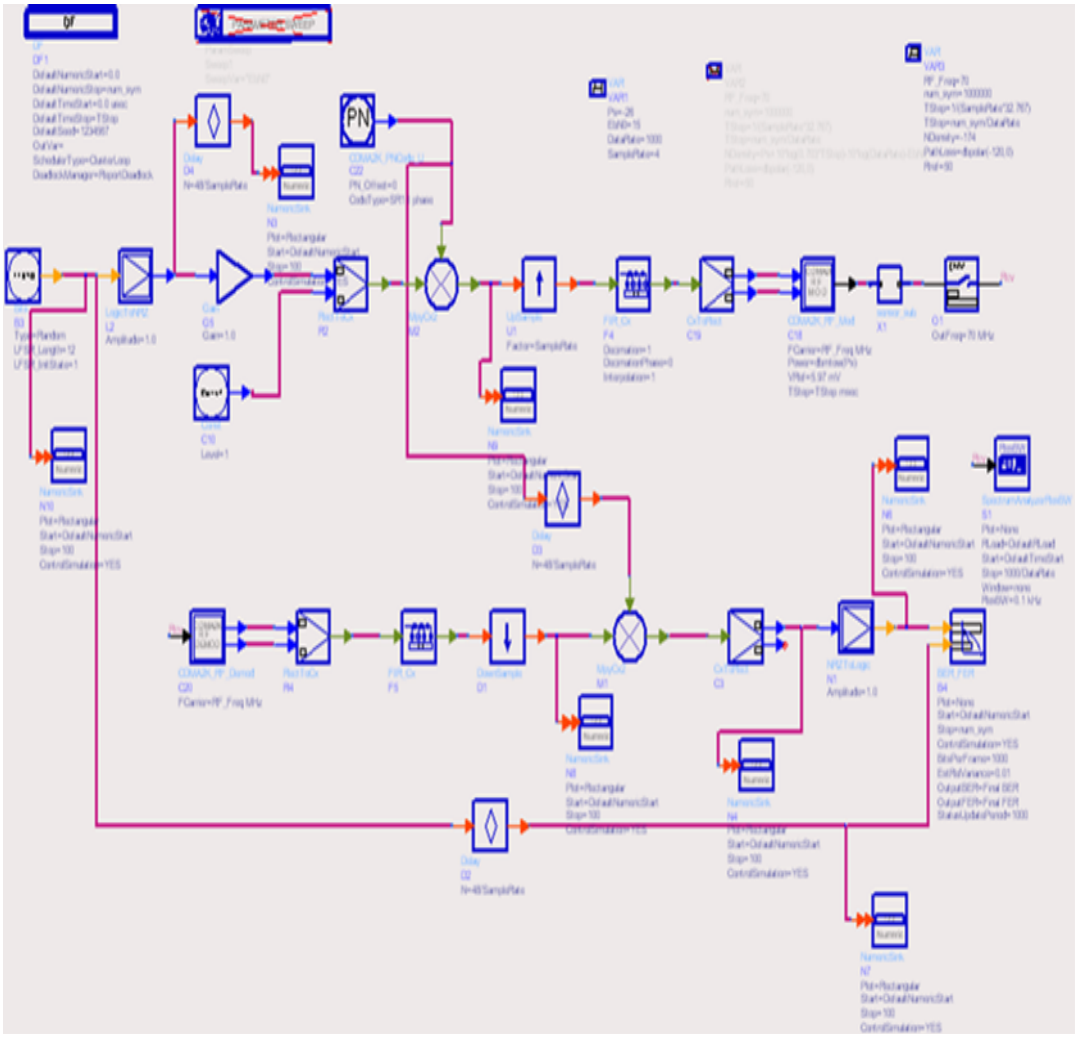

Figure 5.1: ADS TSDF circuit part

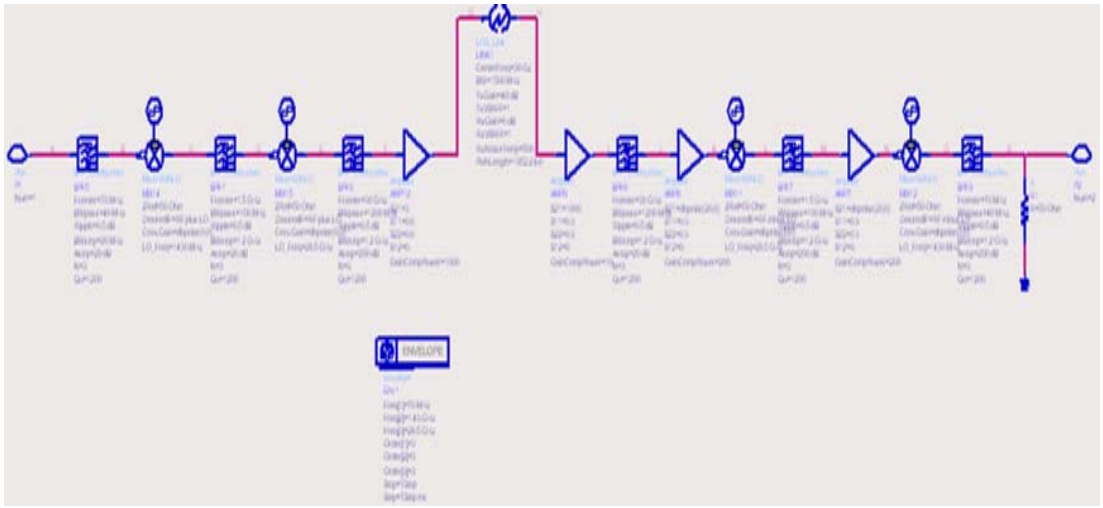

Figure 5.2: ADS Analog RF circuit part

As the communication part in the transmitter starts from the data that needs to be transmitted, the transmitter design started by a source of binary random bits, Figure 5.3, to represent the digital message from the sensing part. Those bits represent the output of (A/D) at the sensor. The generated bits should include the sensor identity, the message and any other required additional bits. The binary random bits generator output is either 0 or 1 with equal probability. The equal probability of 0s and 1s gives the minimum probability of error at the receiver while deciding whether 0 or 1 was sent.

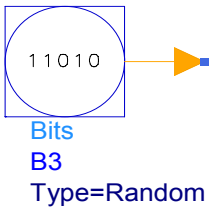

Figure 5.3: Random bits generator

The digital bits are then inserted in a logic-to-non-return-to-zero (LogicToNRZ) converter in Figure 5.4. This component produces the BPSK signal by converting zeros to (– amplitude) and keeping ones (+ amplitude).

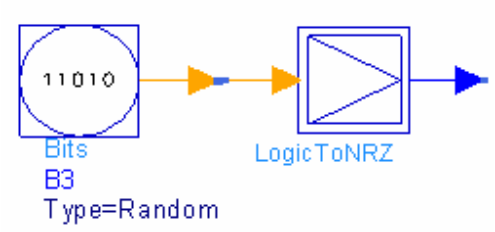

Figure 5.4: BPSK modulator

The signal then is converted from real and imaginary parts to a complex signal using the 'real and imaginary-to-complex converter' (RectToCX) shown in Figure 5.5.

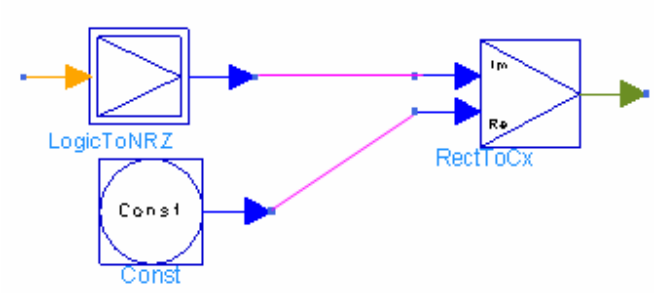

Figure 5.5: Real and imaginary to complex converter

The complex message signal is then spread by a PN sequence and a multiplier. The PN code generator Figure 5.6 generates a PN code with 2^{15}-1 bit M-sequence. The resulting signal will have much wider bandwidth than the original signal. In fact, spreading the message signal will result in a signal with a bandwidth more than the length of the spreading code used.

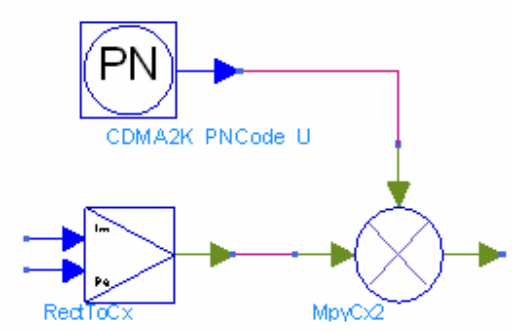

Figure 5.6: Transmitter baseband correlator

After spreading, the data with the new bandwidth is up-sampled at four times the data rate. The operation of up-sampling is done by the insertion of L-1 zeros between every sample of the input signal, where L is the number of samples produced. The data with the new data rate is then filtered by a finite impulse response filter (FIR) as shown in illustrated in 5.7.

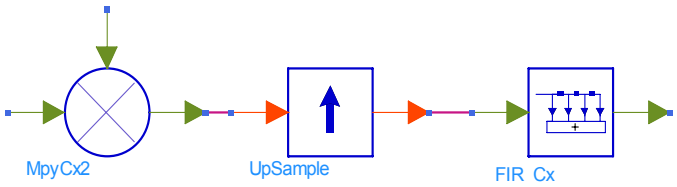

Figure 5.7: Up-sampler and FIR filter

The filtered data is then converted back to real and imaginary parts in order to modulate a carrier of 70 MHz. Two IF stages of up-converting were needed to avoid images. Images are usually filtered using narrow band pass filters. Narrow band pass filters are usually expensive and using them in the sensor was impractical for cost reasons.

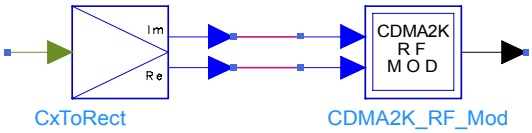

Figure 5.8: Transmitter first up-converting stage

Up to this point, all the components are in the time synchronous data flow (TSDF) schematic of the ADS simulation which deals with components at baseband frequency. The following components work at the RF frequency and so they are in the Analog RF schematic of the ADS simulation.

In the design of both the transmitter and the receiver, each multiplexer is followed by a bandpass filter (BPF) to reject images at undesired frequencies. All the filters used in the whole design satisfied the rule:

$$F_c > 0.02\ BW \qquad (14)$$

where F_c is the center frequency of the filter and BW is the bandwidth of the filter.

In general, filters with a center frequency value less than 0.02 of the bandwidth are either very difficult to build or very expensive, especially at high frequencies. Many filter types are available in the ADS libraries, two of them were the most attractive choices; Butterworth and Chebyshev filters. Based on the fact that Chebyshev filters have a steeper roll-off and more pass band ripple than Butterworth filters do [23], all the filters at the IF and the RF stages were chosen to be Chebyshev filters.

The first filter in the IF stage, which is shown in Figure 5.9, was centered at 70 MHz, which is the frequency of the previous modulated carrier. The bandwidth of the filter should match the data rate of the signal with the chips. The desired bandwidth can be found using the following famous formula for RRC filters [13]:

$$B_{occ} = R_s\,(1+\alpha) \qquad (15)$$

where B_{occ} is the bandwidth occupied by the transmitted signal, R_s is the symbol rate and α is the filter roll-off factor. The 40 MHz came from the (data rate x chips length) (1 + roll off factor), assuming a roll factor of 0.2.

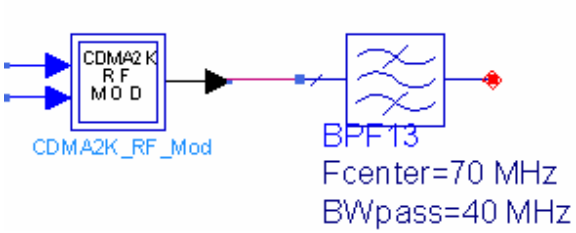

Figure 5.9: Transmitter first IF filter

More than one stage of up-converting was needed for two reasons: to avoid images, and because it is difficult and expensive to built local oscillators and filters at wide bandwidths. The second local oscillator in Figure 5.10 generates a frequency of 1430 MHz to up-convert the signal to a frequency of 1.5 GHz.

The two values for the IF stages frequencies were brought from industry. Most of the RF communication systems use the 70 MHz as a first stage. The second stage usually takes place between 1-2 GHz; this makes the up-converting process more efficient. The

two chosen values supposed to make the fabrication process less expensive by benefiting from the mass production of the components at these frequencies.

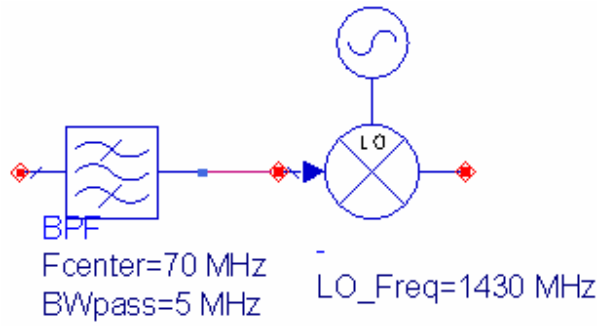

Figure 5.10: Transmitter second up-converting stage

Another BPF centered at 1.5 GHz is used after the local oscillator with 1430 MHz. This filter has to be wider since its center frequency is higher. 100 MHz was chosen as a suitable bandwidth of this filter.

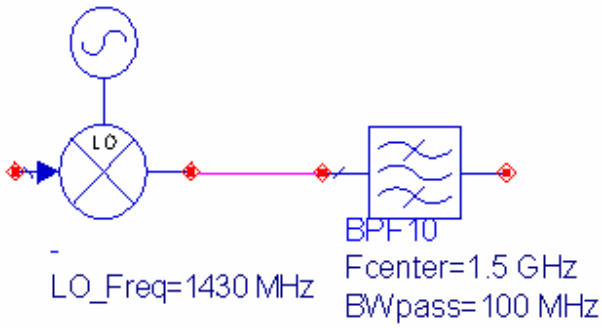

Figure 5.11: Transmitter second IF filter

As the frequency of transmission was set to 30 GHz for the two Ka band antennas, the last local oscillator needed produces 28.5 GHz carrier. This was the last oscillator in the transmitter section since it raised the frequency to the transmission one.
The last filter was set also to the frequency of 30 GHz to make sure that the components at 30 GHz are the only ones to be transmitted.

As the spectrum output components of the last multiplexer will be at (28.5 ± 1.5) GHz, major images from this stage would be at 27 GHz. According to this, the bandwidth of the last filter shown in Figure 5.12 was set to 1200 MHz to be sure to filter out the image component.

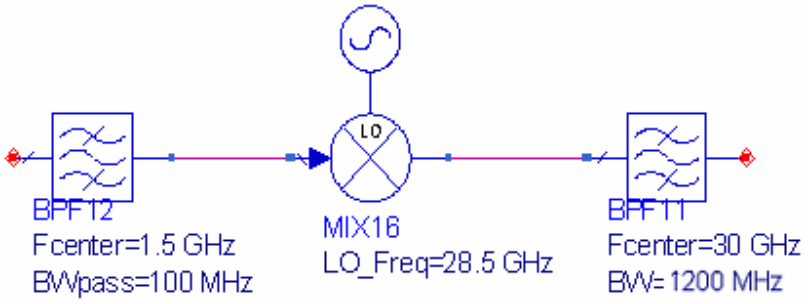

Figure 5.12: Transmitter third up-converting stage

After the 30 GHz BPF, the signal becomes ready to be sent to the satellite. An RF amplifier with 3 dB gain will double the power of the signal and the output will be connected to the phased array antenna input port.

5.2 Propagation

Two satellite LEO links were considered, the 780 km link used by Iridium and the 1410 km used by Globalstar. The same study can be applied to other LEO satellites like Teledesic at 550 km and Orbcomm at 810 km [24]. Using any LEO link other than the 1410 km discussed in this chapter, will result in changing only the transmitted power; increasing if the link is longer than 1410 km and decreasing if shorter.

The link is simulated by a component in ADS called line of sight 'LOS_Link'. As shown in Figure 5.13, the LOS component includes the link information like (path length, bandwidth) and the transmitting and the receiving antennas information like (gain, height above ground, VSWR, efficiency and noise figure or temperature). All these parameters for the transmitting antenna were brought from the ARRAY program and inserted in this component. The 37-element antenna case is considered in this chapter. Assuming worst cases, the transmitting antenna gain used was 17.1 dB, which is the minimum gain in the scanning process. The minimum gain occurred at an angle of 18 degree above horizon, which was the maximum angle of coverage. The slant range of 2977.9 km at 18 degree was calculated using the two relations in [13]:

$$d = r_s\left[1+\left(\frac{r_e}{r_s}\right)^2 - 2\left(\frac{r_e}{r_s}\right)\cos(\gamma)\right]^{1/2} \qquad (16)$$

$$cos\ (EL) = \frac{r_s . \sin(\gamma)}{d} \qquad (17)$$

where d is the distance to the satellite at certain elevation angle (EL), r_s is the vector from the center of the earth to the satellite , r_e is the vector from the center of the earth to the sensor, and γ is the central angel measured between r_e and r_s.

The satellite receiving antenna gain value was assumed to be 20 dB.

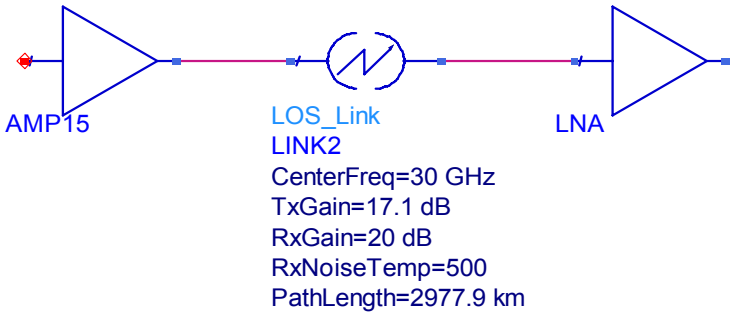

Figure 5.13: Line of sight link

5.3 Receiver

As the receiving part is satellite property, only the needed part of the satellite receiver was simulated. The satellite receiver was designed using all the available parameters and then assuming practical values for all the others. Not all the real numbers used in the existing satellite systems could be borrowed from a real satellite system. While, for example, using typical values for antenna gain, low noise amplifier (LNA), other parameters like filters bandwidths and center frequencies values were set out based on the acceptable communication theories.

The receiver was simulated assuming relative-stationery T_x-R_x. In realty, even if the sensor is stationary, the satellite motion will produce Doppler shift in the received signal. This requires many Doppler bins and signal acquisition techniques. Since none of the mentioned, assuming well-designed, affects the performance of the sensor, they were not included in the simulation to simplify the design and save some simulation running time.

The satellite section started by the receiving antenna implemented in the LOS component. As in any satellite receiver, the first component will be the LNA. The LNA is

a special type of electronic amplifiers used in communication systems to amplify very weak signals captured by an antenna. The LNA used has a 30 dB gain and a system noise temperature of 500 °K is assumed. According to [13], LNA noise temperatures from 30 to 200 °K can be achieved without physical cooling if GaAsFET amplifiers are employed. All the components were considered noiseless except the LNA by setting all noise figures to zero dB and setting the LNA noise temperature to 500 °K. The noise temperature can be related to the noise figure (NF) in linear ratio as follows:

$$NF = 1 + \frac{T_e}{T_o} \tag{18}$$

where T_e is the noise temperature of the device in Kelvins, T_o is the reference temperature used to calculate the standard noise figure – usually 290 °K. Inserting the 500 °K in equation (18) gave a noise figure of 4.4 dB for the LNA.

To compensate for any non-linearity from the LNA, and to reject any other unwanted signals, a bandpass filter, shown in Figure 5.14, centered at the transmission frequency is used after the LNA.

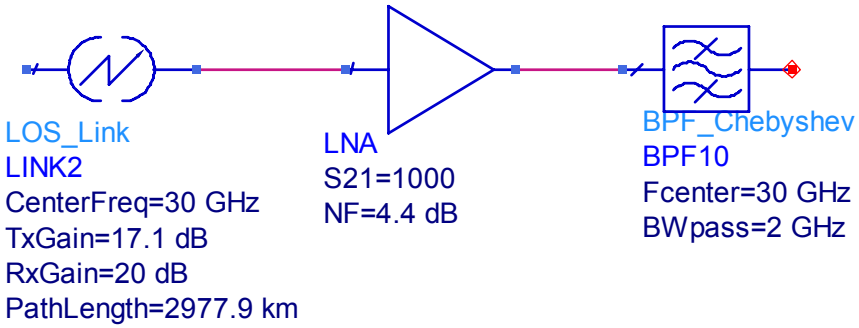

Figure 5.14: Receiver LNA

Each BPF in the receiver is followed by an amplifier to compensate for the attenuation.

The down-conversion process started after the filtration process. The same steps used in the up-conversion in the transmitter are assumed in the receiver but in reversed order. Figure 5.15 shows a local oscillator with a frequency of 28.5 GHz shifts the carrier

down to 1.5 GHz. This local oscillator output is filtered by a BPF centered at 1.5 GHz with 100 MHz bandwidth.

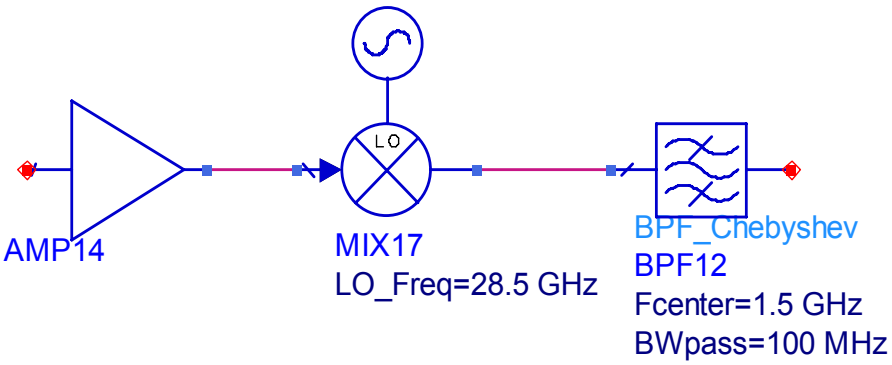

Figure 5.15: Receiver first down-converting stage

The second stage of down-converting, shown in Figure 5.16, is achieved by a local oscillator of 1430 MHz frequency and a multiplier. The output is filtered at the 70 MHz by a 40 MHz wide filter, the bandwidth of this IF filter has to match the data rate of the signal. A wider filter will pass more thermal noise and a narrower one will distort the signal.

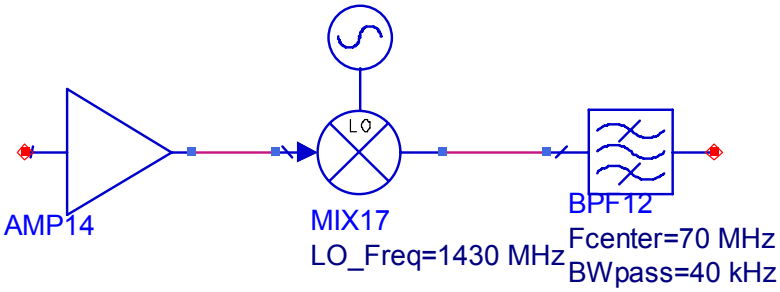

Figure 5.16: Receiver second down-converting stage

At this point of the design, the design process had to go back to the TSDF part and start using the DSP components again.

According to the ADS, a component called 'Envelop Output Selector' has to be used to connect the two schematics as shown in Figure 5.17. An envelope selector 'selects' the spectrum components at the desired IF frequency and then transfers them to the TSDF part. The output of the envelop selector was inserted in two components; a

spectrum analyzer to see the signal in the frequency domain and the CDMA RF demodulator that works as a local oscillator at 70 MHz and a multiplier.

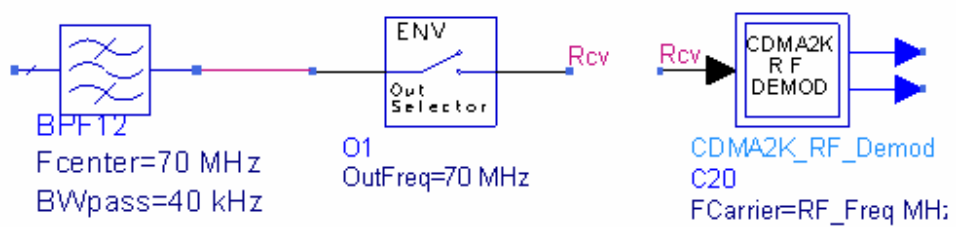

Figure 5.17: Receiver last IF stage

The signal is again converted to complex one and filtered using an FIR filter.

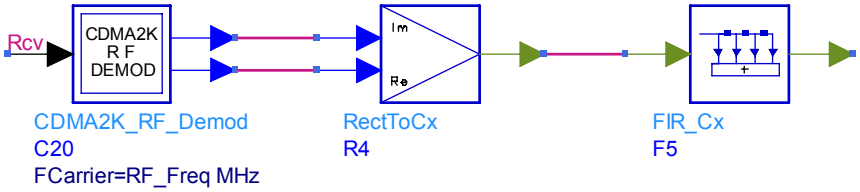

Figure 5.18: Real and imaginary to complex converter

After filtration at the high data rate of transmission, the signal is down-sampled to the original data rate using 'Down Sampler'. This component reduces the sampling rate of its input signal by an integer ratio. Down-sampling is performed by keeping one sample at the output for every four samples in our case at the input [25]. This component does not have a built-in low pass filter (LPF) before decimation. To avoid aliasing, it was necessary to connect a LPF at the input to ensure that the input signal bandwidth is appropriately limited.

For the correlation process, the same PN code generator at the transmitter is used at the receiver. As shown in Figure 5.19, the same M-sequence is applied for coherent detection. The chips sent to the receiver multiplier in the figure are delayed by exactly the time the signal takes from the spreading multiplier to the despreading one. In reality, the satellite receiver knows the chip sequence, and the correlator must be time-synchronized to the received signal.

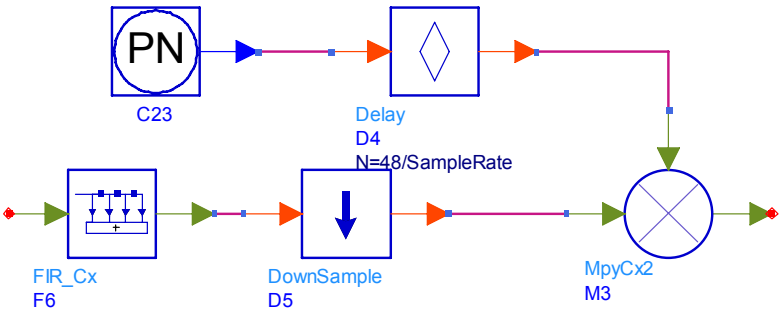

Figure 5.19: Receiver baseband correlator

The signal is then demodulated by a BPSK demodulator or 'NRZ to Logic'. An input ≥ 0 produces an output Logic 1; and an input <0 produces an output Logic 0. The recovered bits out of the demodulator are inserted in a 'Bit Error Rate Estimator' as illustrated in Figure 5.20. This estimator measures the BER (bit error rate) and FER (frame error rate) of a system. In some systems, FER is referred to as PER (packet error rate) or BLER (block error rate). The input signals to the reference (ref) and test (test) inputs must be bit streams. The bit streams must be synchronized; otherwise the BER/FER estimates are wrong. Synchronism is achieved here by the same way it is achieved for the correlation process; a delayed version from the original digital bits, produced by the random binary bits generator was applied to the other input of the BER estimator and the comparison starts between each two bits.

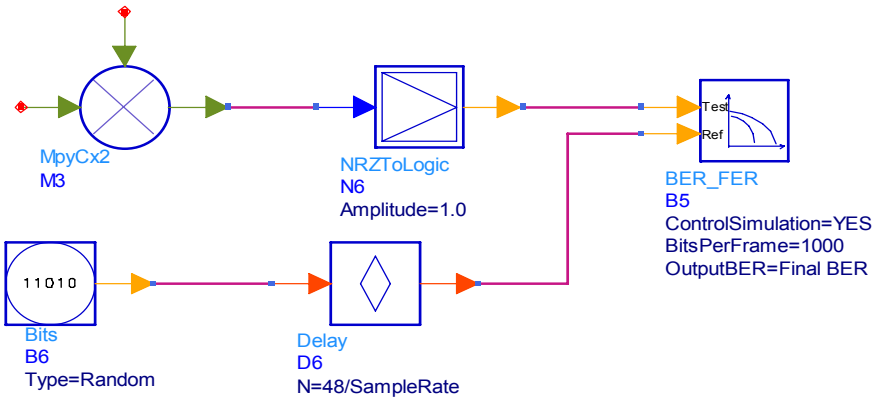

Figure 5.20: BPSK demodulator and BER estimator

The last component was used to evaluate the whole system performance. Next chapter shows the results of one of the cases studied in this thesis.

Chapter 6

Simulation Results and Analysis

6.1 Simulation Results

This chapter shows the results of the ADS simulation which are explained in chapter 5 for the case shown in Table 6.1.

Table 6.1: Link parameters

Sensor:	
Frequency	30 GHz
Data Rate	1000 bps
Code	2^{15-1} bits M-sequence
Antenna	3 cm diameter phased array
Transmitted Power	13.8 μ Watt
Air Interface:	
Satellite Altitude	1410 km
Max Scan Angle	18° above horizon
Satellite:	
Antenna Gain	20 dB/Beam
LNA Gain	30 dB
LNA NF	4.4 dB

This simulation case started with a desired BER $\leq 10^{-5}$. This is considered an acceptable performance for a low data rate of 1000 bps. According to the link budget calculation, the signal-to-noise ratio (S/N) at the satellite receiver input should equal to 10 dB plus the implemented margin. Of course, this is a theoretical value and the real

value will be usually less than that due to the different uncalculated losses and implementation factors.

The spectrum components and the digital bits at each stage are shown next. Figure 6.1 shows a sample of the generated bits at the sensor. The probability of bit value being zero was equal to the probability of bit value being one.

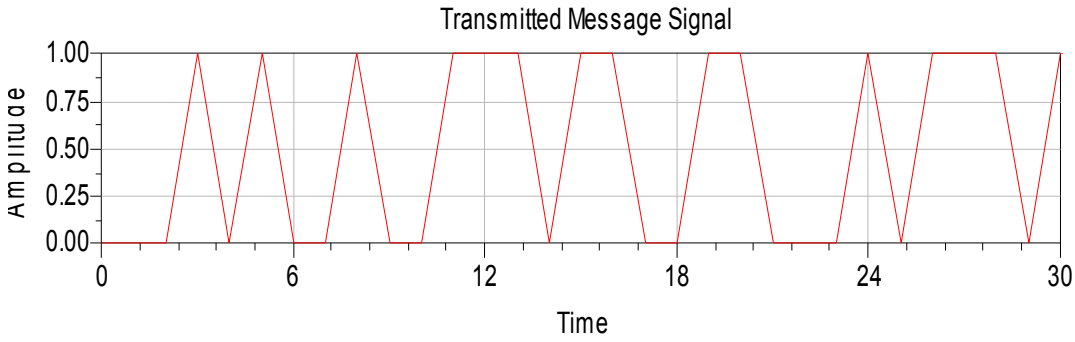

Figure 6.1: Generated random bits

The data then modulated a carrier using a BPSK modulator at the baseband frequency. Each zero produces an output Logic -1; and each 1 stays unchanged as an output Logic 1 as shown in Figure 6.2.

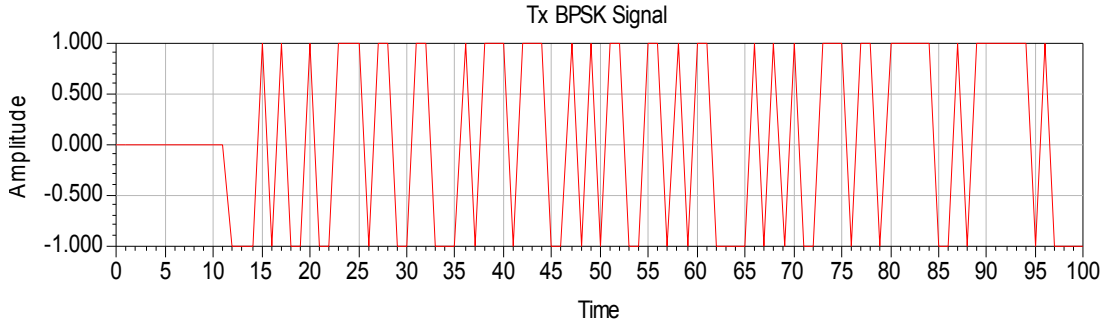

Figure 6.2: Transmitter BPSK signal

The BPSK message is multiplied by high bit (*chip*) rate sequence which results in a stream of *chips*. The RF energy is spread over a wide bandwidth. The resultant bandwidth after spreading is 32.767 MHz which is the product of the M-sequence length and data rate. Figure 6.3 shows the high rate spread signal with the chips.

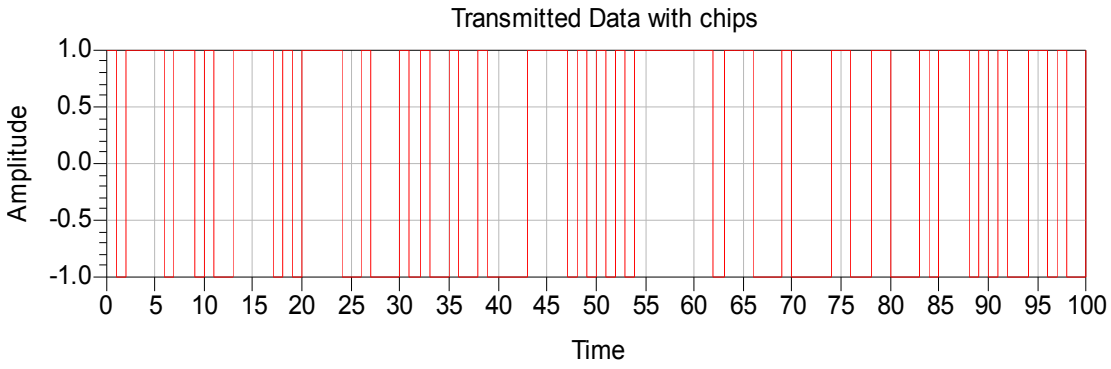

Figure 6.3: Spread signal

The spread signal is then up-converted to the first IF stage at 70 MHz and filtered using 40 MHz filter. The output of the 70 MHz filter is shown in Figure 6.4.

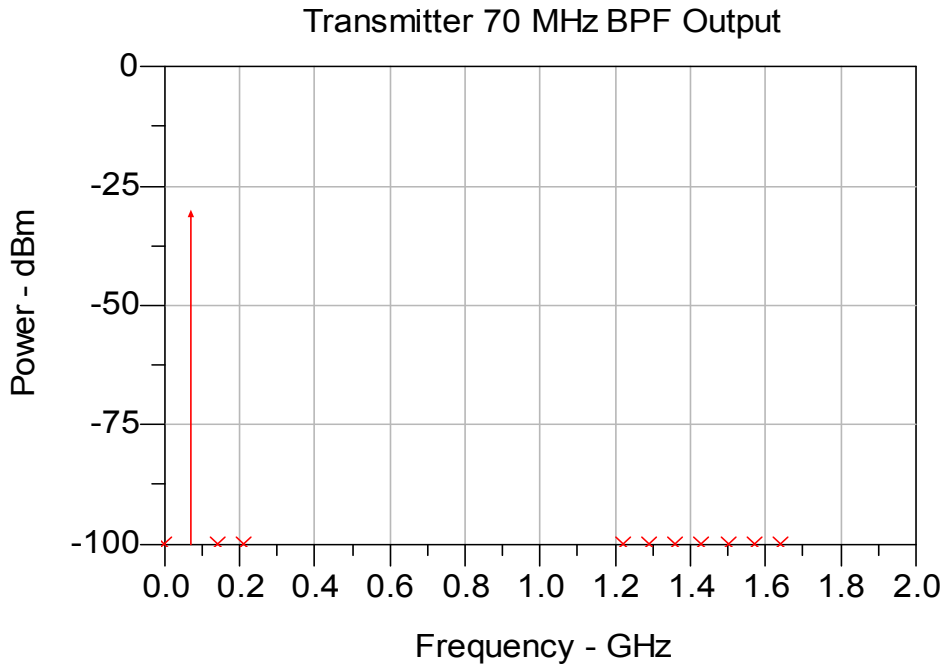

Figure 6.4: Transmitter 70 MHz spectrum

The second IF stage at 1.5 GHz. The signal is filtered by a 100 MHz wide BPF. This non-ideal filter will attenuate the signal and add little noise to the transmitted signal. It is clear in Figure 6.5 that the largest image component is more than 15 dB below the desired one.

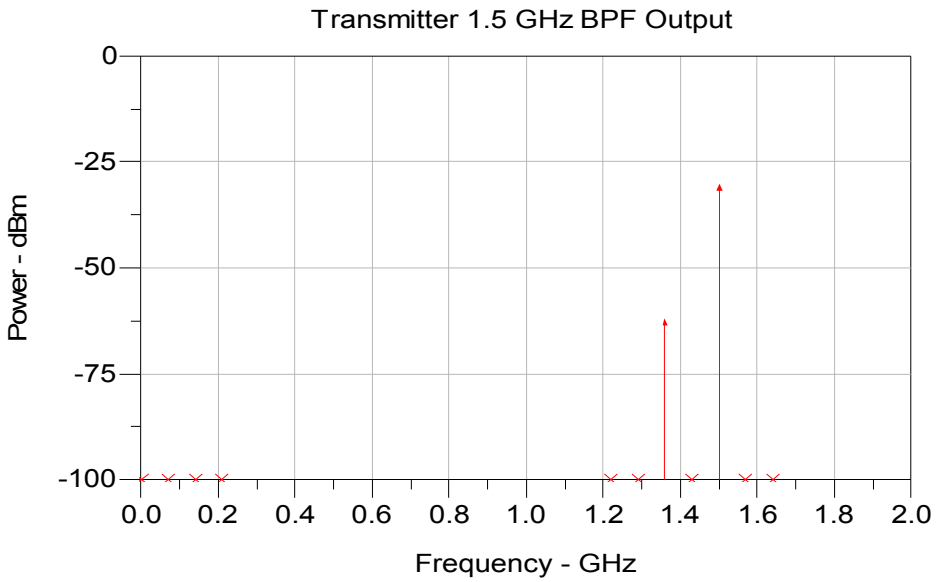

Figure 6.5: Transmitter 1.5 GHz spectrum

Last stage of up-converting delivers a signal at 30 GHz which is ready to be transmitted by the antenna. The signal is up-converted to 30 GHz using a local oscillator of 28.5 GHz frequency followed by a BPF and an RF amplifier. The transmitted signal in Figure 6.6 has 13.8 microwatt or -18.6 dBm.

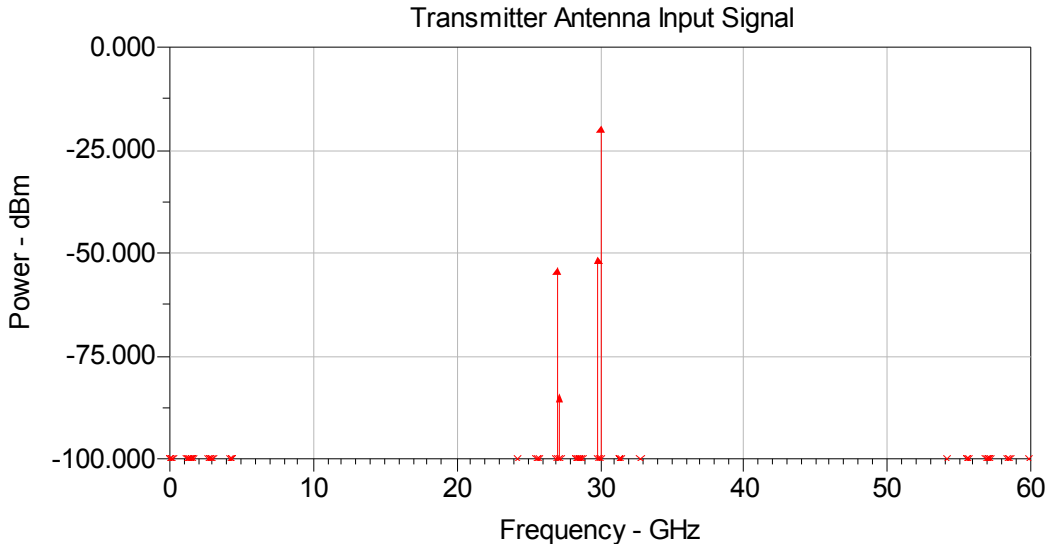

Figure 6.6: Transmitter 30 GHz spectrum

The worst case of transmission, which includes the minimum antennas' gain and the longest link, was assumed. The transmitting antenna lowest gain occurs at the lowest angle of coverage which is 18° in the case of 3.35 cm antenna as listed in Table 4.3. The signal is transmitted by an antenna with a gain as low as 17.1 dB and cuts a link as long as 2977.9 km at elevation angle of 18°. The received signal in Figure 6.7 is almost -173 dBm. The following table shows the attenuations and amplifications that affect the signal power.

Table 6.2: Theoretical link budget for transmitted signal

Signal at Tx Antenna Input:	**-18.6 dBm**
Tx Antenna Gain	+17.1 dB
Path Loss	-191.4 dB
Rx Antenna Gain	+20.0 dB
Signal at Rx Antenna Input:	**-172.9 dBm**

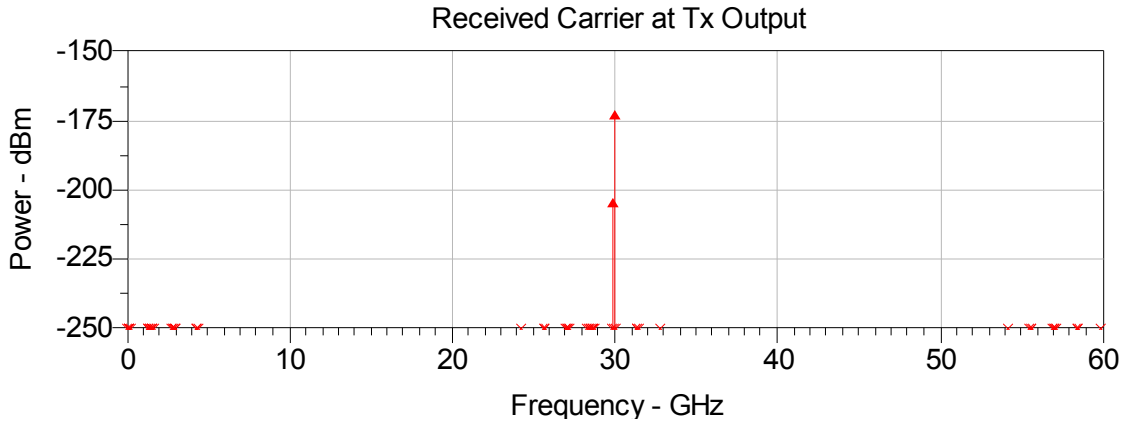

Figure 6.7: Received signal spectrum

Another 30 dB of gain is provided by the LNA. The signal in Figure 6.8 is 30 dB higher than the one in Figure 6.7 at the same frequency. The (C/N) output of the LNA is a major factor in evaluating the performance of the system. The LNA is also considered the major source of thermal noise in the receiver.

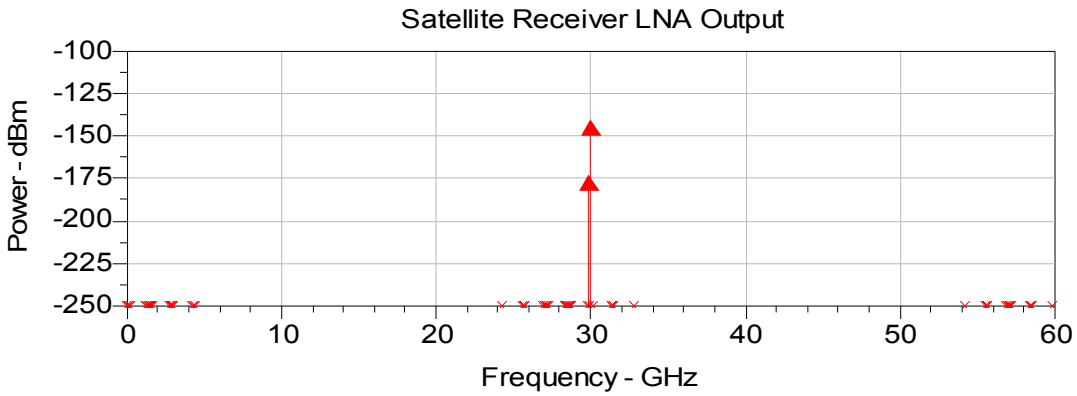

Figure 6.8: LNA output signal spectrum

The signal is down-converted to the first IF stage at 1.5 GHz using local oscillator of 28.5 GHz, BPF centered at 1.5 GHz and 100 MHz wide, and a power amplifier. The signal in Figure 6.9 at 1.5 GHz is more than 50 dB higher than the highest image.

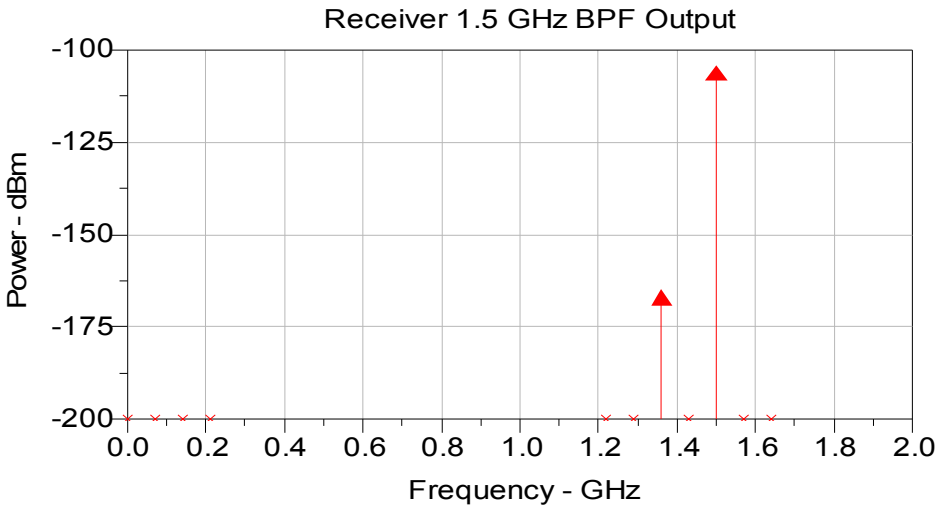

Figure 6.9: Receiver 1.5 GHz spectrum

The second stage of down-converting at the IF stage will shift the carrier down in the spectrum to 70 MHz. The spectrum at 70 MHz was plot using a spectrum analyzer component and is shown in Figure 6.10. The segment time of the spectrum analyzer was set to 1 ms and the bandwidth resolution was set to 100 Hz to get a high sensitivity.

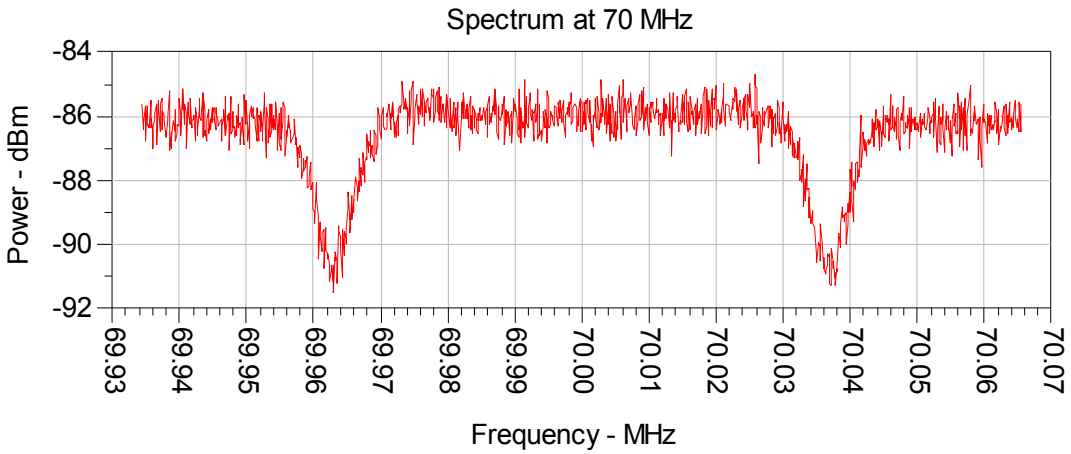

Figure 6.10: Received signal at 70 MHz spectrum

Once the signal gets out of the IF stage in the analog RF section, no additional noise is added to the signal. (C/N) was measured at the IF stages in the transmitter and the receiver and listed in Table 6.3. At the transmitter, the (C/N) ration is 200 dB. That is because of the carrier power. At this high value, the transmitter components up to the IF stage can be considered noiseless. At the receiver last IF stage, the (C/N) ratio is -38 dB, which indicates that the signal is buried in noise. This value changed after the correlation process.

Table 6.3: Carrier-to-noise ratio at Tx-Rx IF stages in dB

freq	cn_in	cn_out
70.00 MHz	200.635	-38.030

Processing starts by down-converting the signal to the baseband stage by the CDMA demodulator. The LPF filter output signal looks like this:

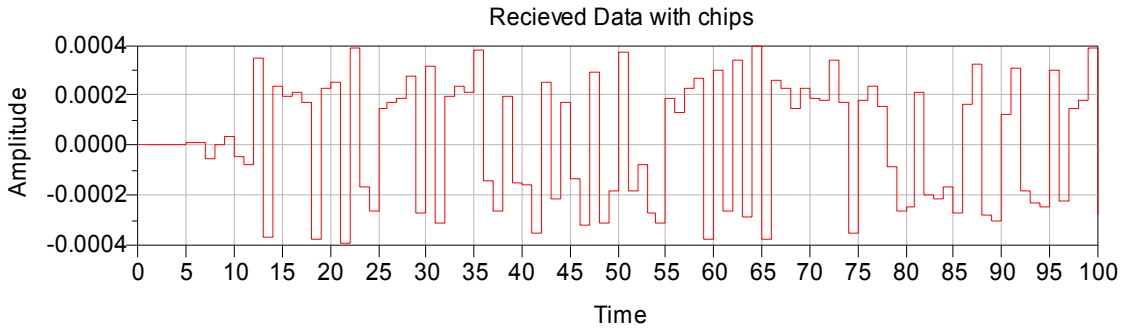

Figure 6.11: Spread signal at the receiver before despreading

As shown in Figure 6.11, the high rate of amplitude changes due to the high chip rate used. After decorrelation with the delayed M-sequence, the signal will go back to the original low data rate as shown in Figure 6.12.

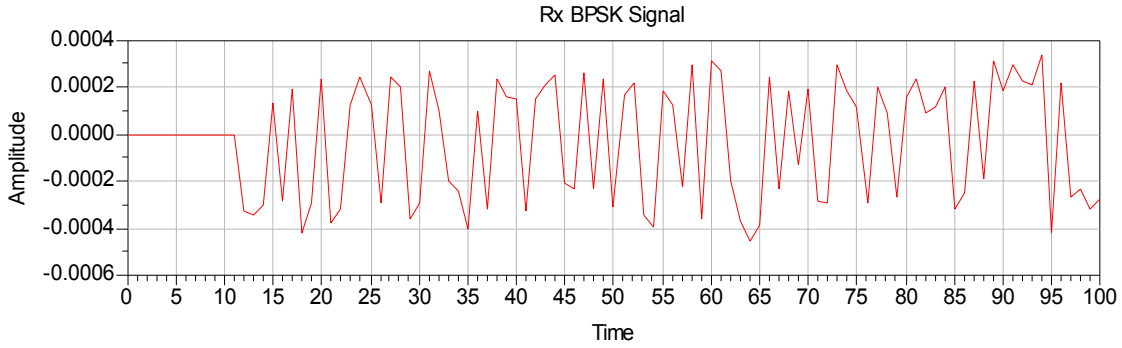

Figure 6.12: Spread signal at the receiver before despreading

The BPSK signal is demodulated using BPSK demodulator and the result is the recovered bits at bit rate of 1000 bps. Below two plots are shown in Figure 6.13, one for the recovered bits and the other one for the delayed original bits. They are almost identical to the point in time they are plotted as the BER is very low.

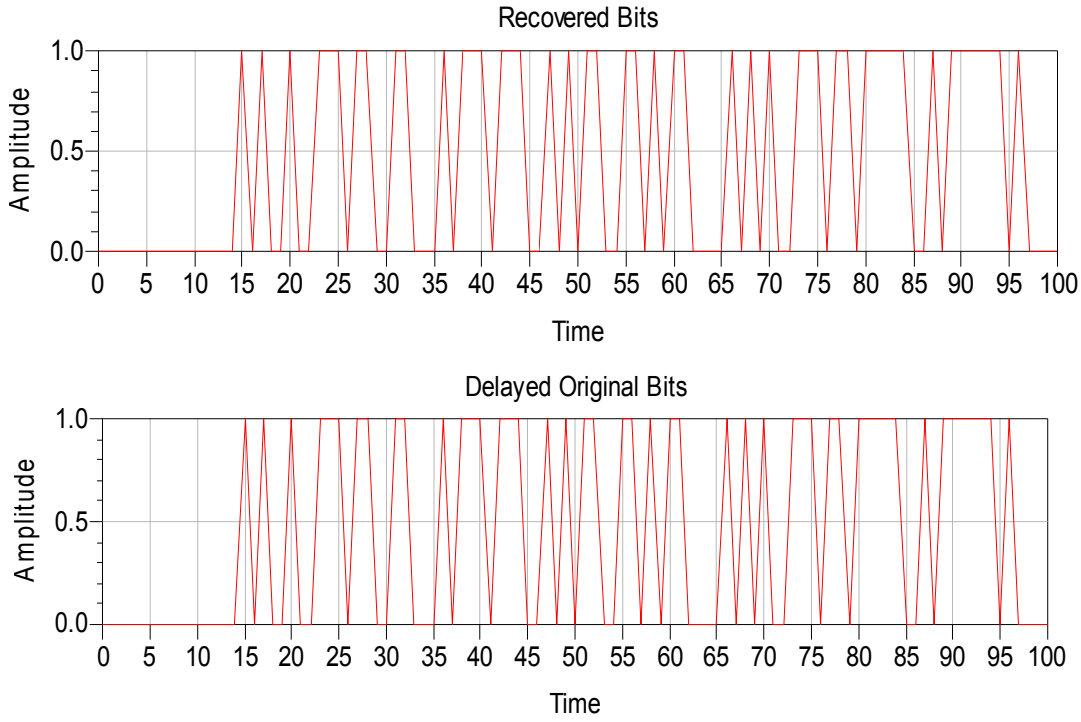

Figure 6.13: Transmitted bits vs. recovered bits

The two samples were inserted in a BER estimator and the resulting BER was around 1.6 x 10^{-4} with BER estimation relative variance of 0.01. The BER value kept changing each time the simulation is run as it is a random variable. In general, the more bits one considers in the estimation process, the more accurate BER one gets. The simulation for the presented case was repeated 15 times. The mean value of the 15 results was 1.632 x 10^{-4}. As the BER was very low, the simulation had to take millions of samples to get accurate results. BER of 10^{-4} means that the simulation finds, in average, an error every 10,000 bit. The simulation at this point was set to average 1000 sample of the received signal. For convenience, the last five simulation results are shown in Table 6.4.

Table 6.4: BER results at Pt = -18.6 dBm

Trial	1	2	3	4	5
BER	1.743 x 10^{-4}	1.477 x 10^{-4}	1.630 x 10^{-4}	1.746 x 10^{-4}	1.675 x 10^{-4}

The resulting BER was worse than the theoretical one as expected. This is due to many factors: many components in the transmitter and the receiver can add noise to the signal; the filters might not have ideal characteristics and the amplifiers nonlinearity. Although a BER of 1.6×10^{-4} is considered enough for this application at data rate of 1000 bps, it was better to increase the transmitted power by few dBs to increase the carrier-to-noise ratio at the receiver and get less errors and a more reliable system.

In order to get the desired performance, 3 dB was added to the transmitted power and the simulation then was rerun. The simulation was again run 15 times. The mean BER was 7.3×10^{-6}. The last five results are listed in Table 6.5. It shows that the BER is around 7×10^{-6} which is better than our goal of 1×10^{-5}. In general, the real performance will be much better as these values are based on the worst case assumptions.

Table 6.5: BER results at Pt = -15.6 dBm

Trial	1	2	3	4	5
BER	8×10^{-6}	9×10^{-6}	7×10^{-6}	4×10^{-6}	5×10^{-6}

The data collection time was increased to 10 times of the previous case because the expected BER is almost 10 times less and the number of bits needed to find errors is larger. The simulation time exceeded 24 hours in the two different transmitted power cases, the reason of why the simulation was run 15 times only for each case.

6.2 Power Source

The choice of power source in this micro-sensor was left open. The power source is a major factor in the design process as it is directly related to the size, life and cost. The application or the manufacturer will determine which one of these three factors is prior. If a reliable source that is able work in any weather is desired, a Lithium battery will be a perfect choice. Lithium batteries can be formed into a wide variety of shapes and sizes so as to efficiently fill available space in the devices they power. They are, in general, lighter than other equivalent secondary batteries [26], and have high energy density, the reason of why they are growing in popularity with the defense and aerospace industries.

If the sensor will be used in an open area where sun light is available most of the day time, a simple solar cell can be used instead of the battery. Using solar cells requires some additional components to store the energy, and they are more probable to be damaged than batteries.

As seen in chapter 5, there are few lossy components in the sensor transmitter such as local oscillators or amplifiers, and the transmitted power in the micro watt range, which tells that the power consumption will be very low and so the choice of power source will not be a limiting factor in the design.

6.3 Spreading Codes

Two spreading codes were suggested for this sensor, Barker Codes and PN codes. Barker codes are short codes and can be found in length of 2, 3, 4, 5, 7, 11, 13 and 23. Codes of length 11, 13 and 23 are used in direct-sequence spread spectrum and pulse compression radar systems because of their low autocorrelation properties. Barker codes couldn't be used in simulating the sensor package as they are not available in the ADS simulation package. Instead Figure 6.14 shows two plots for the coding gain and the resultant needed transmitted power using a transmitting antenna gain of 17.1 dB and the rest of the parameters used in chapter 5. Using the 23-bit code provides 3.2 dB more gain than the shorter 11-bit one. Assuming a data rate of no more than 1000 bps, the required transmitting power does not exceed 15 dBm for the 780 km LEO satellite case and 18 dBm for the 1410 km LEO one.

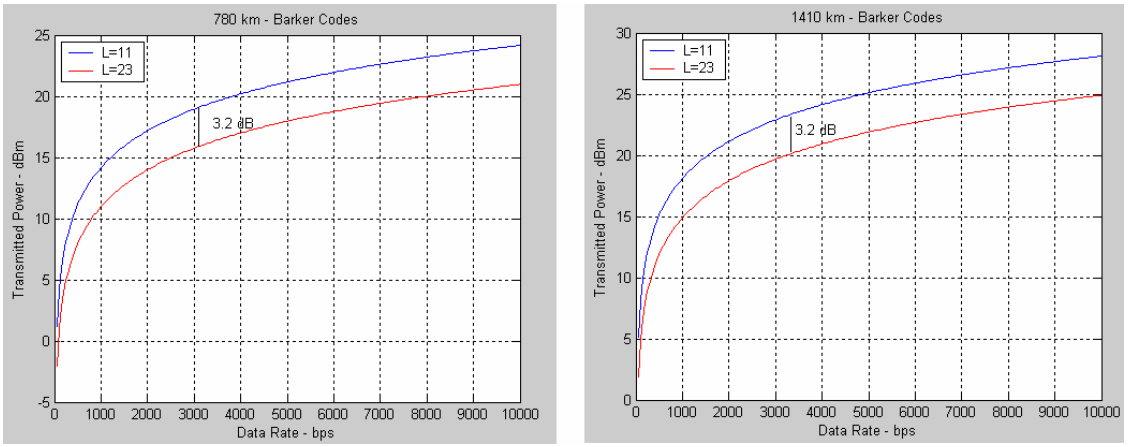

Figure 6.14: 11 and 23-bit Barker code gain – (Left Side) 780 km LEO sat. (Right Side) 1410 km LEO sat

Barker codes main advantage is that they have the lowest autocorrelation sidelobes. A Barker code with N-bits has a peak side lobe of 20 $\log_{10}(1/N)$. On the other side, the main disadvantage of Barker codes is that there are not very many of them which limits the degree of side lobe suppression possible [27].

Pseudorandom sequences have length $N = 2^P - 1$ for some P and generally exhibit side lobes on the order of -10 $\log_{10}$ (N). Figure 6.15 shows the coding gain for PN-sequence with two lengths: 2^{10}-1 chip and the 2^{15}-1 chip which was used in the sensor simulation. The longer sequence shows a 15 dB more gain.

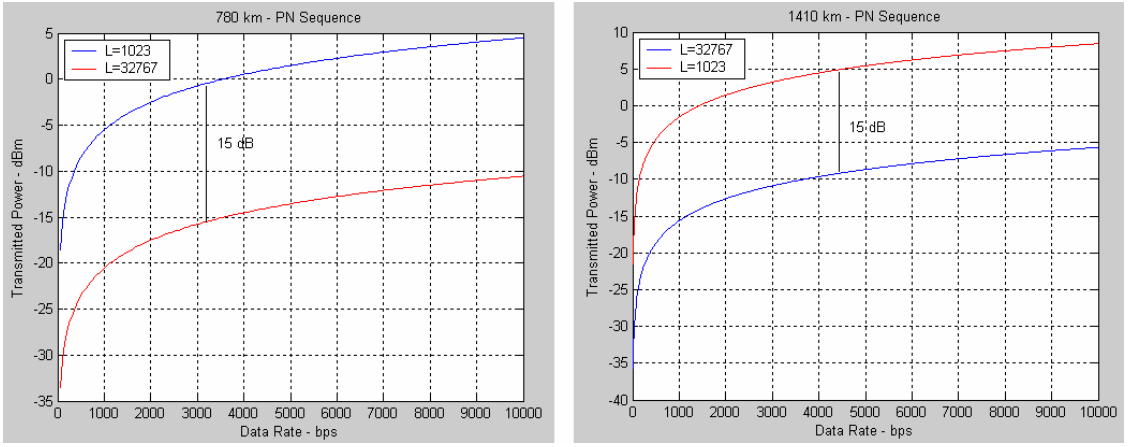

Figure 6.15: 2^{10} and 2^{15}-1 PN sequences gain – (Left Side) 780 km LEO Sat. (Right Side) 1410 km LEO sat

Which code to use is an important decision in the design process. While the Barker codes are easier to implement at both the transmitter and the receiver, they are less secure and provide less gain. The PN codes are more efficient but much more expensive and require a number of shift registers as well as longer processing time.

6.4 Comments on the Fabrication Requirements

The sensor package will be built with the antenna printed on the top surface so that the antenna transmits up-word. The sensor package should have a center of gravity such that when dropped the phased array will be facing up. The best case will be designing the center of gravity so that the top surface for the sensor is exactly parallel to the earth surface. This will assure a high efficient scanning process.

Chapter 7

Conclusions and Future Work

7.1 Conclusions

The simulation results and analysis in this thesis have shown the ability to design a sensor as small as 2.35 cm in diameter that is able to sense different information and send the related data to LEO satellites with very low power and high efficiency. The designed sensor is supposed to have a low cost and provides a reliable link. Using a phased array antenna and DSSS signal reduced the needed transmitted power dramatically.

In the spreading-despreading process, longer codes require longer processing time and more complicated circuitry but provide higher coding gain and more secured link. Code synchronization at the receiver is very important for the security and the correlation efficiency. Using a wrong code or using the right code but with wrong timing at the receiver correlator does not extract the transmitted signal from the noise. Unless the right code with right timing is used to despread the received signal, the output of the correlator will tend to zero. The final BER was always around 0.5 until the exact delay was used at the satellite receiver. Searching a long code such as the 2^{15} -1 bit M-sequence used in the simulation or the other 2^{20}-1 bit M-sequence available in the ADS takes a long time which makes them more secure.

Coverage can be performed by two ways: with a low gain antenna and high transmitted power, or with a high gain antenna and low transmitted power. As shown by the comparison section in chapter 4, using lower frequency bands does not necessarily need using higher transmitted power; the single element at L band needed less power than the two phased arrays at Ka band even that its gain is less by 14.1 and 11.3 dB than the gain of the 37- and the 19-element antennas respectively because the path loss difference can exceed the difference in antennas gain. Phased array antennas have higher gain than typical other antennas. The designed phased arrays showed more than 11 dB higher gain than the single element antenna. Our simulation results show that the larger or the more elements the array is, the higher gain it will have and the narrower beamwidth it will have.

The 37-element antenna gave 3 dB more gain and a narrower beamwidth at all scanning angles than the 19-element antenna did. Narrow beamwidth antennas require more scanning steps than the antennas with wide beamwidth do; so while the 19-element antenna needs 34 scanning steps to cover the space above 12.7°, the 37-element array needs 53 steps to cover 18° above horizon. More scanning steps require more phase shifts and more complexity in the design.

Small RF components are easily fabricated these days using new developed technologies such as MEMS and MMIC. Small phased arrays can be printed at low costs and their phase shifters are no longer complicated or very expensive when using MEMS.

Digital filters play a major role in the system overall performance. Filters should be designed carefully using the standard relationships. ADS simulation of the satellite receiver shows that using filters with wider bandwidth than required will result in more noise at the received signal. On the other side, using filters with bandwiths narrower than required will result in distorted signal at the receiver output. For example, when a BPF of 25 MHz bandwidth was used at the last IF stage at the receiver, the BER exceeded 0.02 because the bandwidth of this filter had to match the data rate of the received signal with the chips, but when a BPF with a bandwidth of 40 MHz was used, which is slightly higher than the data rate of 32.767, the BER rate decreased to less than 10^{-4} using the same parameters. Another way to safely recover the signal at the receiver side was to make redundant versions of it using the up-sampling process. Up-sampling in addition to the spreading process increased the bandwidth of the transmission link dramatically.

The number of filters and RF components affects the power consumption of the sensor; the more components used the more power the sensor consumes. The frequency of transmission sets how many up-converting stages are needed at the transmitter and down-converting stages at the receiver. The more stages used the more images attenuated in both the transmitter and the receiver.

Both simulation tools used, ADS and ARRAY, spend a certain period of time to get the results of each simulation case. Simulation was rerun many times for each case to eliminate any outliers. The results were not identical even though the parameters did not change, but they were close. Longer simulation time gave more accurate results as more samples were taken.

7.2 Contributions

Searching the literature for similar or close work, up to the time of writing this thesis, no similar full design and analysis to microsensors that are able to communicate to satellite orbits was found. Some work, like [11], addressed the major technical considerations of a proposed system but didn't design or discuss the detailed design of the whole system. Other work gave a full design, but for only a part or few parts of the sensor, such as designing the phase shifter required for the sensors that search for the satellites in [28].

The designed sensor package in this thesis represents the first demonstration of a microsensor that uses miniature phased array antenna to access satellite orbits. With no more than 25.7 microwatts (-15.6 dBm) of transmitted power, the designed sensor is expected to deliver data at data rate of 1000 bps at BER less than 10^{-5}.

Using DSSS in the sensor transmission to the satellite orbits is also considered a novel achievement. DSSS has been successfully used in building small sensors transmitting to networks or receiving from satellites, like in [29], but not transmitting to them. The main barrier was the need for high power to access the satellite which would result in a large sensor package.

7.3 Future Work

Future work can include power management protocols, signal processing techniques and, finally, package fabrication. One way that helps consuming the power is using 'Sleep Mode' techniques. It was found that standby modes on electronic devices account for 8% of all British domestic power consumption [30]. Sleep mode has been used widely in small sensors because of the increasing need for smaller batteries or solar cells.

The designed sensor package can also be used in different applications after some modifications. With the aid of the *ultra-wideband* (UWB) technology, the sensor can be used in automotive applications such as collision mitigation, blind spot monitoring and autonomous cruise control (ACC).

References:

[1] B.A. Warneke and K.S.J. Pister, "MEMS for distributed wireless sensor networks," *9th International Conference on Electronics, Circuits and Systems,* vol. 1, pp. 291–294, 2002.

[2] Brett Warneke, Matt Last, Brian Liebowitz and Kristofer S. J. Pister, "Smart Dust: Communicating with a Cubic-Millimeter,"*Computer*, vol. 34, pp. 44-51, 2001.

[3] Federal Standard 1037C. Definition of Phased Array. Accessed April 27, 2006.

[4] M.I. Skolnik, *Introduction to Radar Systems*, 3rd Edition, McGraw Hill Higher Education, New York, NY, 2001.

[5] Josefsson, Persson, *Conformal Array Antenna Theory and Design*, Wiley-IEEE Press, February 2006.

[6] A. Forenza et al, "Pattern Diversity with Multi-mode Circular Patch Antennas in Clustered MIMO Channels," *IEEE Antennas and Propagation Society International Symposium,* vol 3B, pp. 438- 441, 2005

[7] A.K. Verma and Nasimuddin, "Simple and Accurate Expression for Directivity of Circular Microstrip Antenna," *Journal of Microwaves and Optoelectronics*, vol. 2, pp 70-74, No. 6, December 2002.

[8] James R. James, Peter S. Hall., *Handbook of Microstrip Antennas*, INSPEC, Inc.; 2-vol edition, June 1988.

[9] http://www.memsnet.org/

[10] IADC Space Debris Mitigation Guidelines. Inter-Agency Space Debris Coordination Committee (15 Oct 2002). (www.iadc-online.org).

[11] John Hahn. "An application of a disposable remote chemical sensor network," *Digital Avionics Systems Conference*, 13th DASC, AIAA/IEEE, 30 pp. 46 – 51, Oct.-3 Nov. 1994.

[12] Technical correspondence of [11] author with Duracell, Inc., Bethel, Connecticut, on Lithium/ Manganese Dioxide batteries and their power output via FAX, 1994.

[13] T. Pratt, C. Bostian, and J. Allnutt, *Satellite Communications*. Second ed. Hoboken, NJ: John Wiley & Sons, 2003.

[14] C. Decusatis, *Handbook of Applied Photometry.* Optical Society of America, New York.1997.

[15] M. J. Schindler and M. E. Miller, "A 3 bit K/Ka band MMIC phase shifter," in *Microwave and Millimeter-Wave Monolithic Circuits Symp*.Dig., pp. 95–98. 1988.

[16] Gabriel .M. ReBeiz, *RF MEMS: Theory, design and technology*, John Wiley and sons,New Jersey, 2003.

[17] B. Pillans, S. Eshelman, A. Malczewski, J. Ehmke, and C. Goldsmith: "Ka-Band RF MEMS Phase Shifters," *IEEE Microwave Wireless Compon*. Lett., vol. 9, no. 12, pp. 520-522, Dec 1999.

[18] G. L. Tan, R. E. Mihailovich, J. B. Hacker, J. F. DeNatale, and G. M. Rebeiz, "A 4-bit miniature X-band MEMS phase shifter using switched-LC networks," *IEEE Int. Microwave Symposium,* vol. 3, pp.1477-1480, Philadelphia, PA, June 2003.

[19] Jigang Liu, Ronghui Wu, Qingxin Su: "A direct up-conversion transmitter architecture for TD-SCDMA handset," *Personal, Indoor and Mobile Radio Communications, 2003. PIMRC 2003. 14th IEEE Proceedings.* vol 3, pp. 2900 – 2904, 7-10 Sept. 2003.

[20] Gong Shaofang, M. Karlsson , A. Serban: "Design of a radio front-end module at 5 GHz," *Emerging Technologies: Frontiers of Mobile and Wireless Communication, 2004. Proceedings of the IEEE 6th Circuits and Systems Symposium.* vol. 1, pp. 241 – 244, 2004.

[21] Agilent Technologies, Agilent EEsof EDA Library, ADS 2007-11-09.

[22] Agilent Technologies, Agilent Ptolemy Simulation Manual, Sept 2002.

[23] Daniels, Richard W. (1974). *Approximation Methods for Electronic Filter Design*. New York: McGraw-Hill.

[24] Michel Capderou, *Satellites: Orbits And Missions Springer*; 1 edition, April 29, 2005.

[25] Down Sampler, "Numeric Components," *ADS 2006A*, *Agilent Technologies.* September 2006.

[26] Buchmann, Isidor (March 2006). BatteryUniversity.com: Charging lithium-ion batteries. Cadex Electronics Inc.

[27] M. Richards, *Fundamentals of Radar Signal Processing,* McGraw Hill Publishing, 2005.

[28] Y.J. Ko, J.Y, Park, J.U, Bu: "Integrated 3-bit RF MEMS phase shifter with constant phase shift for active phased array antennas in satellite broadcasting systems," *TRANSDUCERS, Solid-State Sensors, Actuators and Microsystems, 12th International Conference*. vol 2, pp.1788 – 1791, 8-12 June 2003.

[29] J.F. Diouris, M. Clenet, A. Sharaiha: "An experimental multisensor receiver for DS/CDMA system," *Signals, Systems and Computers, 1996. 1996 Conference Record of the Thirtieth Asilomar.* vol 1, pp. 60 – 64, 1996.

[30] "TV standby buttons will be outlawed," Times UK Online, 2006-07-12.

Vita

Mohammad AL-Saleh was born in Amman, Jordan. He received his B.S. in Telecommunication Engineering from Yarmouk University, Irbid, Jordan in 2005. He enrolled in Virginia Tech as a graduate student in 2006 at the National Capital Region campus in Falls Church, Virginia and graduated in the Fall semester of 2007. Upon graduation he will start an internship with Qualcomm Inc in San Diego, California before going back to start his Ph.D. This thesis fulfils the requirements for his M.S. in Electrical Engineering.